1.

FINAL TECHNICAL REPORT

NASA GRANT NAG8-190
(and extended by NAG8-1077)

STUDIES OF PLANETARY SCALE WAVES AND INSTABILITIES IN SUPPORT OF THE GEOPHYSICAL FLUID FLOW CELL EXPERIMENT ON USML-2

by

J. E. Hart
Department of Astrophysical, Planetary and Atmospheric Sciences
University of Colorado, Boulder, 80309

May 30, 1995

ABSTRACT

High resolution numerical simulations of thermal convection in a rapidly rotating channel with gravity perpendicular to the rotation vector are described. The convecting columns are subject to a β-effect resulting from cross-channel topographic vortex stretching. The symmetries of the problem allow many invariant wavenumber sets, and this property is associated with the existence of stable multiple-equilibria at modest supercriticality. The transition to chaotic behavior involves the production of intermittent unstable orbits off a two-torus in energy space. At very high Rayleigh number (of order 10^6 to 10^7) the motion can be turbulent, depending on the size of β. However, the turbulence is usually characterized by an almost-periodic formation of patches of small scale convection that cause regular pulsations in the accompanying strong zonal jets. The processes maintaining these flows may be related to those responsible for the zonal currents on Jupiter and for cyclic variability on the Sun.

0. OVERVIEW

The Geophysical Fluid Flow Cell (GFFC) experiment is scheduled to fly on board the USML-2 mission in September 1995. In support of this flight, and to generate ideas for experiments to be conducted, we have carried out an extensive modeling study of thermal convection confined to an equatorial annulus. This is a reasonable model for the nonlinear dynamics of quasi-two-dimensional "banana" cells, i.e. the convection modes observed on the SL-3 flight of the GFFC. Of great interest are the questions of how the banana cell states become chaotic, whether or not mean zonal flows can be generated, and what the nature of the turbulent states are. To this end we have constructed models that are relatively simple to integrate (as opposed to GCM type simulations that are out of the question for the GFFC parameter ranges and timescales). This report describes the major modeling results, and focuses on interesting discovery of exotic pulsating turbulent states that will be sought during the USML-2 mission.

1. INTRODUCTION

One of the outstanding problems in geophysical fluid dynamics is the origin of zonal winds on the giant planets and differential rotation on the Sun. Busse (1976, 1983) proposed that the Taylor-Proudman constraint associated with a strong basic rotation would cause the interior motions of rapidly rotating planetary atmospheres to be invariant along the rotation axis. In Boussinesq gas or liquid models the resulting two dimensional convecting columns were found to be subject to a number of secondary instabilities (Or and Busse, 1987, hereafter OB87, for free boundaries; Schnaubelt and Busse, 1991, Schnaubelt, 1992, for rigid boundaries). One is a mean flow instability in which convecting columns, tilting in the zonal and radial directions, produce Reynolds stresses that generate a zonal shear flow. This zonal shearing motion is capable of further tilting the cells, leading, in principle, to large mean flows as the dissipation is reduced.

A crucial effect in Busse's model is the stretching, by the curvature of the planetary atmosphere, of radially displaced convecting columns aligned with the rotation axis. The standard model configuration is an equatorial annulus or zonally periodic channel with sloping ends and gravity perpendicular to the basic rotation vector (figure 1). The slopes generate a topographic β-effect which provides a mechanism for travelling Rossby waves, as well as a tendency for chaotic behavior at modest Rayleigh number. In this paper we study the spontaneous generation of strong zonal jets at high Rayleigh number. If β is either too small or too large, the motions are either lack such jets, or are stable altogether. We call the intermediate regime, with dominant zonal currents and various forms of turbulence, β - convection. Although the geometry and vertical structure of the Boussinesq model is highly simplified, the results are relevant to scaling arguments of Ingersoll and Pollard (1982) for deep convection on the giant planets. These order of magnitude estimates rely, in part, on the low Rayleigh number computations of Lipps (1971) for ordinary 2-D convection in an imposed shear flow. As the presence of vortex stretching associated with the β-effect can have a dramatic influence on the structure of both low and high Rayleigh number situations, it is of interest to charac-

terize the possible states through a sequence of numerical experiments.

Thompson (1970) proposed a type of mean flow instability as an explanation of the 4-day retrograde rotation of the Venusian atmosphere. His model was criticized by Lilly (1971) who argued that on Venus there is no constraint to guarantee pure transverse convecting rolls that have the necessary strong interactions with a zonal shear flow. In the Busse scenario such a constraint is provided by the basic rotation. Laboratory experiments on Boussinesq-liquid spherical shells using outward centrifugal buoyancy (Carrigan and Busse, 1983) and electrostatic radial buoyancy (Hart et. al, 1986) confirmed the validity of this idea over a fairly wide range of Rayleigh and Taylor numbers. However, the latter study showed that increasing the Rayleigh number at fixed Taylor number invariably leads to a breakdown of the columnar "banana cell" convection as the Taylor-Proudman constraint is modified by buoyancy forces parallel to the basic rotation vector. The breakdown first occurs at high latitudes, then gradually erodes down into the equatorial banana cell region as the Rayleigh number increases. Thus one question is whether or not there is a parameter range for β-convection with very strong mean zonal flows and self-consistency in the sense of low local Rossby number and negligible thermal winds.

There have been a number of studies of the evolution of columnar β-convection with increasing Rayleigh number, addressing the question of the transition from steadily propagating thermal Rossby waves, which arise at the linear stability boundary for the onset of convection, to more complicated spatio-temporal forms. For application to planetary atmospheres and the solar rotation problem, a model should produce a relatively large zonal flow in which the columnar convective eddies do not dominate the total streamfields. For example, the data from Voyager (Ingersoll, et al., 1981) show fluctuating velocities at cloud levels on Jupiter which are considerably smaller than the zonal-mean jet speed at most latitudes. However, all the weakly nonlinear models of β-convection constructed to date have eddy kinetic energies either far exceed the zonal means. Highly truncated models have been pushed to large Rayleigh number where rough equivalence can be found, but the use of low truncation at high supercriticality is suspect. In both cases strong regular-wave patterns at modest wavenumber are found that are not easily associated with features imbedded in the clouds on the giant planets, nor in photometry or helioseismology of the solar atmosphere. All these objects nonetheless boast a strong latitudinally varying differential zonal rotation (Howard and Harvey, 1970, Ingersoll et al., 1981).

Lin, Busse and Ghil (1989), hereafter LGB89, used a perturbation method to study mode mixing and transition, ostensibly near the neutral curve for linear instability. Their model predicted two "multiple" states with the same waveset symmetry but differing amounts of zonal cell tilt with radius. Transition to chaotic time dependence was via a period doubling cascade at near-critical Rayleigh number. Lin (1990) used a truncated Fourier expansion to suggest that the convecting column system might be subject to a sideband "double column" instability in which rows of like-sign vortices would align permanently on the same side of the model channel, leading to large mean flows at modest Rayleigh numbers. A period doubling cascade was predicted at low supercriticality in this latter work as well. It is not

clear that these results are robust with respect to model truncation. The well-known failure of severely truncated models of two-dimensional convection and baroclinic instability to predict the outcome of highly resolved simulations at even modest supercriticality has motivated us to revisit the thermal Rossby wave problem. In our high resolution calculations we find significant differences in the transition scenario compared to the low-order models, as well as some unusual turbulent states. There are internally-consistent turbulent regimes with large zonal jets that may either be quasi-steady or almost-periodic, depending on β.

The rest of this report is organized as follows. The basic model equations and numerical methods are summarized in section 2. Section 3 describes our results on multiple equilibria and the transition to chaos. Section 4 presents data from a number of runs at large Rayleigh number with various values of the β parameter. Our main conclusions are summarized in section 5.

2. MODEL EQUATIONS AND METHOD

Our central motivation is to shed light on the nonlinear dynamics of β-convection in the simplest geometry that has been universally used in the previous modeling studies mentioned above. The basic model is derived for flow of a Boussinesq liquid in a rectilinear channel whose cross-section is shown in figure 1. The governing equations are obtained by perturbing off a state of geostrophic balance (Busse and Or, 1986). The Rossby number for the flow, $\bar{U}/2\Omega D$ or, as an even stronger condition, $\omega^*/2\Omega$, is assumed small. Here $\bar{U}$ is the rms flow speed in the x-y plane, Ω is the basic rotation rate, D the channel width, and ω^* is the local vertical vorticity. The motions are then essentially two-dimensional in the x-y plane and controlled by the quasi-geostrophic vorticity equation (c.f. Pedlosky, 1987), with the one addition that zonal (x) variations of the relatively weak y-directed buoyancy forces can generate "vertical" vorticity (i.e. vorticity aligned with the rotation axis). In order to maintain horizontal non-divergence of the lowest order velocity field in the x-y plane, the component of buoyancy in the y-direction is assumed small compared with the Coriolis deflection of the zonal u velocity. The thermal winds associated with horizontal temperature gradients and the component of gravity along the axis of rotation that would be present in a spherical atmosphere are neglected. In order to be self-consistent with lowest order geostrophy, the nonlinear vortex stretching term in the vertical vorticity equation is neglected with respect to planetary vortex stretching. These scaling assumptions are re-examined a' posteriori in section 5. Finally, while topographic slopes are used to generate a β-effect, all the boundaries are assumed to be free-slip. If the sloping surfaces are almost flat, the lowest order fields do not require Ekman layers to adjust the normal shear of the horizontal velocities at these surfaces to zero. Thus there will be no Ekman suction damping, and lateral diffusion of heat and momentum is the only dissipative mechanism included.

When lengths are scaled by D, velocities by νD^{-1}, temperature relative to a background conductive state by $\nu\kappa^{-1}\Delta T$, and time by $D^2\nu^{-1}$, the governing vorticity equation and the heat equation become (following LBG89):

$$\frac{\partial \omega}{\partial t} + J(\psi,\omega) - \beta \frac{\partial \psi}{\partial x} = - Ra \frac{\partial T}{\partial x} + \nabla^2 \omega \ , \tag{1}$$

$$P_r \left\{ \frac{\partial T}{\partial t} + J(\psi,T) \right\} = \nabla^2 T - \frac{\partial \psi}{\partial x} \ , \tag{2}$$

with

$$\omega = \nabla^2 \psi \ , \tag{3}$$

$$u = - \frac{\partial \psi}{\partial y} \tag{4}$$

and

$$v = \frac{\partial \psi}{\partial x} \ . \tag{5}$$

The parameters are defined by:

$$\text{Prandtl number } P_r = \frac{\nu}{\kappa} \ , \tag{6}$$

$$\text{Rayleigh number } R_a = \frac{g\alpha \Delta T D^3}{\kappa \nu} \ , \tag{7}$$

$$\beta \text{ - parameter } \quad \beta = \frac{4 \tan(\eta) \Omega D^3}{L\nu} \ . \tag{8}$$

Here α is the coefficient of thermal expansion, ν the kinematic viscosity, and κ the thermal diffusivity. Other parameters are defined in figure 1. This paper studies flow regimes in the R_a - β plane at a fixed value of P_r = 1.0.

The β parameter as given in (8) is related to the topographic slopes in figure 1, which in turn follow from extracting a slot from a full sphere and assuming that the motions extend along the axis of rotation all the way through the interior. This was the canonical view proposed by Busse (1983). However it is important to observe that eqn. (8) is identical in magnitude to the β parameter obtained for shallow to moderately deep convection between spherical shells separated by a distance H, measured along the axis of rotation, when H is small compared to a full sphere radius R_s. Under the local slope approximation for a slot of width D intersecting the surface of a sphere of radius R_s at latitude θ, the ratio of the change in depth across the slot to the average depth is

$$G = \frac{\delta h}{h} = \frac{2\Omega D^2 \beta}{\nu} = \frac{D \cos(\theta)}{R_s \sin^2(\theta) \left\{ 1 - \frac{H}{R_s \sin(\theta)} \right\}} \tag{8'}$$

where the last term in brackets is absent for columnar convection extending all the way through. Since the column length L (or H) only appears in β, the results for a given β apply equally to shallow or moderately deep as well as to full interior-crossing Boussinesq convection.

The above system is solved numerically by a pseudospectral algorithm. The expansion functions are chosen such that stress-free, impermeable, and infinitely conducting boundary conditions are satisfied on the vertical walls at y = 0 and y = 1. We write:

$$\psi = \sum_{m=0}^{\infty} \sum_{n=1}^{\infty} \psi_{m,n} \sin(n\pi y) \exp(imx) , \tag{9}$$

$$T = \sum_{m=0}^{\infty} \sum_{n=1}^{\infty} T_{m,n} \sin(n\pi y) \exp(imx) , \tag{10}$$

Then, the boundary conditions mentioned above,

$$\psi = \frac{\partial^2 \psi}{\partial y^2} = T = 0, \quad \text{at } y = 0,1,$$

and periodic zonal boundary conditions are automatically satisfied. The above representation assumes that the zonal periodicity length is 2π times the channel width. This particular aspect ratio is maintained throughout the paper. The solutions are affected if the aspect is significantly smaller so that the lowest wavenumber corresponds to tall thin cells. Linear stability analyses of finite-amplitude β-convection in an infinite channel (Schnaubelt, 1992) predict sideband instabilities with maximum growth rates for wavenumbers corresponding to $m \simeq 1$ in a 2π long channel. Thus our choice of this particular aspect ratio is expected to capture the essential physics of flows in longer channels while maximizing computational efficiency.

The numerical method is a Fourier spectral collocation scheme based upon a truncation of (9) and (10). The variables ψ and T of configuration (physical) space are mapped back and forth into the coefficients $\psi_{m,n}$ and $T_{m,n}$ of spectral space using fast Fourier transforms. The time integration of equations (1) and (2) is performed semi-implicitly. An implicit Crank-Nicolson formulation (Smith, 1965) is used for the linear terms, whereas an explicit three-level Adams-Bashforth scheme (Richtmyer and Morton, 1967) is adopted for the nonlinear terms. The Crank-Nicolson step is unconditionally stable and therefore the timestep for the linear parts is restricted solely by requirements of accuracy. However, the explicit scheme for the nonlinear parts requires a timestep that satisfies the Courant-Friedrichs-Lewy condition for numerical stability.

Products of the variables are evaluated in configuration space to avoid computationally expensive convolution sums of the phase space variables. However, all other calculations are carried out in phase space,

where derivatives reduce to simple multiplications by powers of the wavenumbers. Aliasing errors are removed using the so-called 2/3 dealiasing rule. The pseudospectral code allows initial conditions to be random fluctuations in any required wavenumber set, or the results of a previous simulation. It was thoroughly tested against linear analysis, simple nonlinear examples, and (by setting $\beta = 0$) against previous two-dimensional Rayleigh-Benard results (e.g. Moore and Weiss, 1973). The results presented below are believed to be convergent on the basis of obtaining quantitatively similar solutions at double the spatial resolution. The higher Rayleigh number runs used 256 (x) and 65 (y) modes. A typical run of 200,000 timesteps takes about a day on an IBM RS6000-320 workstation, or a couple of hours on a CRAY-YMP.

3. MULTIPLE STATES AND THE TRANSITION TO CHAOS

We start by summarizing a large number of computational runs at moderately supercritical Rayleigh numbers designed to illustrate the types of secondary instability involved in the transition to chaos. We also show that in this intermediate R_a region of parameter space between linear instability and full turbulence there are at least two locations where linearly stable multiple solutions are found. All the results reported in this section are for $P_r = 1.0$ and $\beta = 2800$, to permit comparisons with previously published works on this problem that have concentrated on these particular values.

As a point of reference, figure 2 illustrates the behavior of the primary instability. The linear versions of (1) - (2) have solutions with ψ and T proportional to $\exp(st + i\alpha x)\sin(n\pi y)$. The growth rates for $P_r = 1$ are then given by the quadratic

$$s^2 + s\left\{2k^2 + \frac{i\beta\alpha}{k^2}\right\} - \frac{\alpha^2 R_a}{k^2} + k^4 + i\beta\alpha = 0 \ , \tag{11}$$

with $k^2 \equiv n^2\pi^2 + \alpha^2$. From this one can easily determine the critical curve where Re(s) crosses the imaginary axis. This occurs at a frequency

$$\omega = \frac{-\alpha\beta}{2k^2} \tag{12}$$

and a critical Rayleigh number

$$R_{ac} = \frac{k^6}{\alpha^2} + \frac{\beta^2}{4k^2} \ . \tag{13}$$

Figure 2a shows that the critical Rayleigh number and wavenumber both increase with β, (as $\beta^{4/3}$ and $\beta^{1/3}$ respectively, for β large). At supercritical conditions the wavenumber of maximum growth is smaller than the critical wavenumber (e.g. compare figures 2a and 2b for $\beta = 20000$). In our calculations the x-wavenumber $\alpha = m$ is an integer quantized by the zonal periodicity. For $P_r = 1.0$ and $\beta = 2800$ the critical values are $R_{ac} = 30{,}830$ at $\alpha_c = m = 9$ and $n = 1$. The critical Rayleigh number for $n = 2$, $m = 9$ is slightly bigger (36,254), but as n increases beyond 2 the critical Rayleigh number

increases rapidly (for n = 3 it is about 67,000) and the associated critical wavenumber first decreases then increases. Over the whole parameter plane $0 < R_a < 10^8$, $0 < \beta < 10^6$ the n = 1 mode has the highest linear growth rate, although as β becomes very large a wider and wider range of n's have roughly the same growth rate. This leads to the important question of finite-amplitude meridional (i.e. cross-channel) scale selection.

Nonlinear solutions of (1)-(2) can be found with certain invariant wavenumber subsets based on zonal and cross-channel periodicity, and on a form-preserving shift-reflect symmetry. It is obvious that any solution with initial zonal wavenumbers confined to m = 0 (the zonal component of the flow), m = M (the "fundamental wave"), and all zonal harmonics of M, will not scatter energy into any other zonal wavenumbers. Solutions based on dividing the zonal periodicity length by some integer M thus preserve the initial sparse (for M large) spectral occupation matrix, though they may be unstable to perturbations in longer wavelengths. For example, OB87 study linear perturbations to finite amplitude solutions in an infinite channel with various values of M around 8, and find supercritical sideband instabilities with long wave excitation in wavenumbers smaller than one. Similar comments can be made with respect to the cross-channel periodicity (for these boundary conditions). However, we do not find stable finite-amplitude solutions with a fundamental cross-channel periodicity N > 1, though they certainly exist.

Invariant wavenumber sets with only even values of n + m in (9) and (10) are also possible (OB87). These are related to motions in the channel that are preserved under a reflection about the mid-line y = 0.5, and a translation in x by one half the fundamental M^{-1} periodicity length. In the nonlinear solutions studied here we label various end-states based on their fundamental zonal periodicity M, and whether they have the shift-reflect symmetry or not. Asymmetric A-states have both even and odd values of n + m, while S-states have n + m even only. In addition, it is useful to note that some states, while filling low wavenumbers, still have peak energies at a fairly large value of m. Figure 3 shows spectral occupation diagrams for several different states and illustrates our nomenclature. Finally, every solution has a companion reflected about the midplane under $y \rightarrow 1 - y$ alone, and/ or shifted by an arbitrary phase in x. The simplified geometry with uniformly sloping ends does not provide enough asymmetry to determine the sign of the zonal flow at y = 0, for example, and this, as well as the eddy positions in x, are determined by initial conditions. The above symmetries are often found in such 2-D channel models. Some examples are ordinary sheared convection, Howard and Krishnamurti (1986), baroclinic instability on the f-plane, Cattaneo and Hart (1990), and thermosolutal convection, Moore et al. (1991), among others. Because of the β-effect our problem does not share the left-right $x \rightarrow -x$ reflection symmetry that these latter systems have. In addition it is useful to note that the shift-reflect symmetry S-states will be lost in more general geometries such as cylinders, spherical shells, bodies with non-conical ends, etc. As shown below, S-modes participate in the low Rayleigh number bifurcations, but are unstable at suitably high forcing.

Figure 4 summarizes the results of about 100 runs with $P_r = 1.0$ and $\beta =$

2800. At slightly supercritical values of R_a, the system equilibrates to a type 9S symmetric state, as expected from linear theory. At a value of R_a slightly smaller than 35,000 this 9S state becomes unstable to the 9A mode, consistent with the finite amplitude stability calculations. Or and Busse (1987) call this symmetry breaking instability a "mean flow instability", because the interaction of zonally phase-shifted even and odd cross-channel modes with the same zonal wavenumber can generate an m = 0 zonal flow component. LBG89 give examples of multiple equilibria following the bifurcation to an asymmetric state. Only one asymmetric type 9A solution was found in the present computational exercise. The phase shift between the first and second cross-stream mode of the fundamental zonal wave is 130 degrees at R_a = 35,000. This corresponds to "Solution I" of LBG89, that has a phase shift of "$\chi \simeq 120^o$". We attempted to start a 9A solution at Rayleigh numbers near 35,500 with an initial phase shift of 15° and relative amplitudes given by LGB89 for their "solution II". However the system typically evolved to a singly periodic mean flow state with $\chi \simeq 130^o$. This corresponds to the vacillating solution I of LGB89. Based on our limited and potentially protocol-sensitive study of this issue, we suspect that there is only one asymmetric solution at near critical conditions.

The asymmetric 9A state bifurcates to an amplitude-periodic 8A state at R_a = 37,500. OB87 showed that the mean flow secondary state (i.e. 9A) would almost immediately (upon increasing R_a) suffer a sideband instability, but they did not find any tertiary steady convection states. Thus we believe the 8A limit cycle to be a simple extension of the 9A periodic-state similar to the so-called vacillatory convection solution calculated by OB87 for R_a near 40,000 at low resolution (triangular T5 truncation; retaining only modes with $n + m < 6$). Because they did not consider finite aspect ratio channels, the comparison cannot be made more exact. The similarities suggest that periodic amplitude modulation of the convection, as seen in the limited resolution model of LGB89 and the $O(10^2)$ degree of freedom calculations of Schnaubelt (1992), is a robust feature of this problem.

However, there is simultaneously a regime of stable steady convection following the instability of the mean-flow 9A mode, that has, however, the 1A(7) symmetry. This nonlinear fixed-amplitude tertiary travelling wave state is a result of the sideband instability. The 8A and 1A branches coexist for a substantial range of R_a. Initial value problems with small 1A perturbations to the 8A state indicate that it is stable up to $R_a \simeq 60{,}000$ which is close to the onset-value for totally desymmetrized chaos. Each integration at increasing R_a along the 1A branch is essentially subject to a 1A perturbation (i.e. the previous solution), and so is at least linearly stable until a transition is made to another type of time dependence or waveset symmetry.

Previous studies have cited evidence for period-doubling cascades to chaos. At high resolution, completed cascades of this type are not found. The 8A state undergoes a single doubling at R_a = 57,500, but then a further bifurcation to a torus occurs in a narrow window centered on 75,500, before chaotic motion ensues for $R_a > 76{,}000$. Figure 5 illustrates this transition. Note that the single period-doubling occurs at much higher values of R_a than that found from highly truncated models with period doubling ($R_a \simeq$ 36,000, LGB89, Lin 90), indicating that previous studies used insufficient

resolution to explore the actual transition to chaos. OB87 also found period doubling in this range, but used somewhat different boundary conditions having free-stress eddies, but periodic zonal flows. It is not known whether the differences between our calculations and theirs are due to boundary conditions or to truncation. In our 8A transition, the initial high frequency mean-flow vacillation is eventually replaced by a low-frequency motion that has its origin in the toroidal bifurcation to modulated vacillating convection. Figure 6a shows that the limit cycle behavior is related to a periodicity in the tilt of the convection cells that drives an oscillating zonal flow. This is largely a result of a periodic phase shift in x of the even and odd cross-stream fundamental modes, giving rise to a sort of interference vacillation. At larger R_a there is a nearly-periodic pairing of like sign vortices on opposite sides of the channel (e.g. figure 6b panels 5 and 13), due to the relative drift of the row of vortices at the top of the channel with respect to those at the bottom. This is reminiscent of the truncated solutions of Lin (1990) where rows of n = 2 vortices propagate relative to each other along opposite walls at modest R_a. Lin predicted that the like-sign vortices would permanently position themselves near the opposing boundaries as R_a is further increased, in a process that was called a "double column" instability. The solution in figure 6b might more appropriately be called an n = 2 differentially-drifting-column (DDC) state. Similar vacillations were predicted by Schnaubelt (1992) in situations with curved ends, giving a y-varying β parameter. He found oscillatory instabilities of steady convection with the DDC signature. The DDC vacillation appearing here at high R_a does not require sidebands or curved boundaries for its existence. The intermittent excursions off the torus (figure 5c) are suggestive of a tangent bifurcation. Physically they seem to be related to almost periodic pulsations of the zonal flow - convection system, which, because of small scale high-frequency fluctuations, can occur irregularly in time.

For completeness we note that the 1S state undergoes a similar transition to chaos, though at lower R_a . Referring to figure 4, the steady 9S mode first suffers a sideband instability in which the new the spectrum is dominated by wavenumber m = 9. With increasing R_a the spectrum flattens out and the flow makes a transition to aperiodicity at a low Rayleigh number, $R_a \simeq 43{,}750$. Figure 7 emphasizes that there is no period doubling, and the frequency separation in the quasi-periodic states is not large. Because they are unstable, both the 1S and the 8A transition branches are not physically significant.

For $R_a > \simeq 62{,}500$ the only stable state is 1A(6). The chaotic branch overlaps with a steady solution in a narrow window between 59,500 and 62,500. The steady solution is dominated by wavenumber 7 and has much weaker sidebands than the wavenumber 6 dominated chaotic solution at the same R_a. Figure 8 shows typical streamfunctions and zonal wavenumber spectra for these modes. The spatial spectra of the 1A chaotic branch, though dominated by m = 6 near $R_a = 60{,}000$, rapidly become filled in at low wavenumbers as R_a increases. We could not track the 1A chaotic state back in Rayleigh number to find its origin. At $R_a = 59{,}500$ it loses stability to a 2A periodic state, that in turn becomes unstable to 8A at slightly lower R_a.

4. HIGH RAYLEIGH NUMBER FLOWS

The zonal (m = 0) component of the flow over the regime diagram of figure 4 does not exceed the eddy velocities and is generally rather small. It is of interest to explore larger Rayleigh numbers to identify parameter values where one might get substantial zonal jets. We begin with a cut in β at $R_a = 10^6$, $P_r = 1.0$. Some typical streamfunction vs. time images are shown in figure 9. These solutions are obtained from desymmetrized initial conditions (type 1A), and all but panels a) and b) remain asymmetric.

At $\beta = 0$ one recovers steady non-chaotic roll convection dominated by wavenumber 1. A small ($O(10^3)$) value of β leads to steady travelling convection, with waves travelling from left to right in response to the deepening of the channel in y. β's of this magnitude produce weak mean flows with space-averaged mean kinetic energy $\bar{K}$ much less than the eddy kinetic energy K'. Near $\beta = 6000$ there is a narrow window of hysteresis between travelling convection with almost-steady amplitude and weak mean flows connected to the $\beta = 0$ ordinary convection branch, and a chaotic strong-jet jet solution that is connected to the turbulent β-convection branch. The hysteresis spans a β range of several hundred (see also fig. 14). As β is further increased the dominant wavenumber of the convection grows, but it remains substantially less than that expected from linear theory. Figure 10 shows the relation between nonlinear wave selection and the fastest linearly growing wave for the same conditions. The difference is biggest at low β where the flows are most supercritical. The largest zonal flows are found on the low β side of the chaotic domain, and in this region the zonal circulation is quasi-steady. When β is increased almost-periodic vacillations of the zonal shear flow and the heat flux across the channel are observed (figure 11).

Figure 12 shows total stream and temperature fields (less the conduction profile), which are typical of flows at extreme R_a. The associated time series of zonal energy, pointwise zonal velocity and heat flux are shown in figure 13. The zonal flow is built up rapidly during a period of violent and small scale (because β is large) convection. When the zonal shear reaches its maximum the convection is suppressed and the zonal jet relaxes slowly back to low values and the process starts over. The relatively slight aperiodicity of this almost-periodic large scale system appears due to the irregularity and patchiness of the small scale turbulent convection that arises when the shear is small. The cycling is consistent with the idea of mean flow instability and rapid zonal shear growth as the convection turns on, followed by the relatively quick suppression of the convective plumes when the shear becomes too large (we recall that linear stability results show stabilization of transverse roll convection by a strong vertical shear). An important point is that the zonal shear relaxation time is roughly independent of β and R_a (see figures 11 and 13 and table 1), and therefore this turbulent flow vacillation occurs on the viscous D^2/ν timescale. Once the convection shuts down, the zonal jets decay on this long time scale. The mechanism for these cycles appears to be different from the mode-mixing interference vacillations at low R_a (i.e. fig. 6b).

TABLE 1
CHARACTERISTICS OF β-CONVECTION

β	R_a	N_u-1	$\bar{K}$	K'	ΔU	$K'\bar{K}$	τ
0.0	5×10^5	15.1	0	2×10^6	-	-	-
4000	"	7.1	2.8×10^3	8.7×10^5	22	6.3×10^4	-
4500	"	4.5	1.8×10^3	5.6×10^5	76	2.3×10^4	-
4500	"	4.3	1.3×10^5	9.9×10^4	702	8.4×10^5	.12
5000	"	1.9	1.1×10^5	5.4×10^4	654	4.2×10^5	.12
1.0×10^4	"	1.4	1.5×10^4	4.0×10^4	163	1.4×10^5	.12
1.5×10^4	"	1.0	2.3×10^3	6.3×10^3	64	2.8×10^4	-
0.0	1×10^6	19.1	0	4.9×10^6	-	-	-
4000	"	16.4	3.5×10^4	4.2×10^6	17	7.6×10^5	-
6000	"	9.1	5.6×10^3	2.1×10^6	25	2.1×10^5	-
6000	"	5.4	6.2×10^5	1.6×10^5	1526	3.2×10^6	-
8000	"	1.8	1.9×10^5	6.9×10^4	880	1.1×10^6	.12
1.5×10^4	"	.77	5.1×10^4	1.5×10^4	479	2.7×10^5	.08
2.0×10^4	"	.51	2.3×10^4	7.1×10^3	326	1.2×10^5	.08
2.8×10^4	"	-	2.0×10^3	5.4×10^3	12	4.0×10^4	.06
2.8×10^4	5×10^6	3.67	9.6×10^4	3.4×10^6	224	2.7×10^6	.08
3.5×10^4	"	1.59	5.6×10^5	4.1×10^5	1588	2.6×10^6	.07
5.0×10^4	"	1.05	2.4×10^5	4.4×10^4	1056	1.5×10^6	.12
7.5×10^4	"	.47	7.2×10^4	1.6×10^4	577	4.1×10^5	.09
1×10^5	"	.26	1.4×10^4	6.3×10^3	252	7.3×10^4	-
4.0×10^4	1×10^7	3.7	1.7×10^5	7.6×10^6	315	9.4×10^5	.07
4.5×10^4	"	2.3	1.8×10^6	1.7×10^6	2839	1.1×10^7	.10
5.0×10^4	"	1.8	1.5×10^6	1.8×10^6	2581	6.4×10^6	.10
7.5×10^4	"	.93	6.9×10^5	1.7×10^5	1803	3.1×10^6	.08
1.0×10^5	"	.73	3.3×10^5	5.4×10^4	1264	1.6×10^6	.07
1.5×10^5	"	.33	6.3×10^4	1.5×10^4	552	3.1×10^5	-

$\underline{Nu}$ - 1 = x and time average of w'T' at y=0.5.
$\bar{K}$ = global and time average of zonal kinetic energy (m = 0.)
K' = global and time average of eddy kinetic energy (m ≠ 0).
$\Delta\underline{U}$ = time average of zonal cross-channel velocity difference.
$K'K$ = space-time average of eddy to zonal kinetic energy production rate.
τ = dominant period of zonal kinetic energy fluctuation.
(shorter run times lead to uncertainties in some lines of the table)

Figures 14, 15 and table 1 summarize the situation. As R_a increases a window in β opens up where large zonal jets can be found. Quasi-steady zonal currents occur on the low-β side of the window, while almost periodic jets occur in the middle. At fixed R_a, increasing β causes a drop in the convective flux N_u - 1, along with a concurrent decrease in the eddy kinetic energy. The zonal kinetic energy first rises then falls, and the largest values of the shear $\Delta U/D$ seem to occur when the eddy and zonal kinetic

energies are roughly the same, especially at high R_a. However, there are many states with $\overline{K}$ substantially greater than $\overline{K'}$ and these occur as β moves towards, but is not too close to, the linear stability boundary. Further discussion follows in section 5. We have not taken the extremely small steps in β needed to explore the high Rayleigh number $\beta \rightarrow \beta_{lin}$ transition in detail, as simulations of these low-friction motions require high spatial resolution and small timesteps.

5. DISCUSSION AND CONCLUSIONS

We have studied two-dimensional thermal convection aligned with the axis of basic rotation in a β-plane channel of aspect ratio 2π having free slip sidewalls. The computations had unit Prandtl number. The main conclusions are:

i) The fundamental single-wave state, which arises from the linear instability of the conductive thermal profile for β less than

$$\beta_{lin} = \left\{ \frac{4R_a}{3} \right\}^{3/4} , \qquad (14)$$

equilibrates at wavenumber 9 (18 cells in the zonal direction for $\beta = 2800$). As the Rayleigh number is increased at fixed β, this finite-amplitude steady convection suffers successive secondary instabilities to an asymmetric (mean flow) steady state, and then to a vacillatory mean flow state at a slightly lower wavenumber (8). This follows the scenario of Or and Busse (1987), who first performed linear stability analyses of the finite-amplitude supercritical steady states.

ii) The vacillatory motion, including only wavenumber 8 and its harmonics, becomes chaotic at about twice the critical Rayleigh number via a quasi-periodic 2-torus scenario. The two-frequencies seem to result from a tilted cell interaction and a phase-winding instability of the first two cross-stream modes. Earlier studies (Lin et al. 1989, Lin 1990) that predict a transition to chaos by period-doubling at about 20 percent supercriticality may be inaccurate due to truncation. Another possible cause for the difference may be related to the finite aspect ratio geometry with its associated wavenumber discretization.

iii) Only 1 steady asymmetric form of convection was found at slightly supercritical Rayleigh number. The zonal phase relations between the first two cross-stream wavy modes suggest that this state is consistent with the "Solution I" weakly-nonlinear perturbation results of Lin et al. 1989. The absence of their "Solution II" may be a result of our numerical protocol.

iv) For $40{,}000 < R_a < 60{,}000$, and $\beta = 2800$, several linearly stable finite amplitude states coexist. These include a periodic wavenumber-8 (plus harmonics) state, a periodic wavenumber-2 (plus harmonics) state, and a steady asymmetric state with all wavenumbers excited. This last mode is

the most important because of its association with the high Rayleigh number fully desymmetrized turbulent flows.

v) For Rayleigh numbers up to 10^7 the most vigorous zonal jets induced by the convection can be found in parameter space along the long-dash line of figure 15. This is approximately given by

$$\beta_V \simeq \left\{ \frac{R_a}{7} \right\}^{3/4} . \qquad (15)$$

For $\beta < \beta_V$ the amplitude of the zonal velocity falls rapidly, and is zero when $\beta = 0$. In this region the motions are weakly chaotic in a band with β slightly less than β_V, becoming steady in amplitude for β less than about $0.5\ \beta_V$. This latter value is a crude estimate based on a coarse sampling in this area of parameter space. Along the β_V curve the dominant zonal wavenumber of the convection is one or two, and the zonal flows are quasi-steady with small but irregular fluctuations associated with the high-frequency structure in the convection.

For $\beta > \beta_V$ the dominant wavenumber of the convection increases and the zonal flows begin to pulsate on a diffusive timescale. The small scale convection is highly turbulent, especially at our extreme value of $R_a = 10^7$. However, the oscillation of the zonally averaged quantities is nearly regular.

Along a curve very crudely given by

$$\beta_m \simeq .013\ R_a \qquad (16)$$

the ratio of the time-averaged zonal kinetic energy to the time-averaged eddy kinetic energy is a maximum, with values of about 2.5 at $R_a = 5 \times 10^5$ and over 6 at $R_a = 10^7$. It is doubtful that β_m intersects the linear stability boundary (14) though it is probable that the turbulent pulsating states occur closer to β_{lin} as R_a is increased beyond 10^7. As β is increased above β_m at fixed R_a the convection shifts to still higher wavenumber and eventually dies out as the neutral curve (14) is crossed.

If R_a is increased at fixed β (as in section 3), curve (15) is eventually crossed and the chaotic convection at smaller R_a becomes regular again. This process is distinct from the relaminarization found in low order models that give steady convection following an inverse period-doubling cascade at fixed wavenumber as R_a crosses about 40,000 at $\beta = 2800$ (LGB89). Here the chaotic high-mean-flow states at $\beta = 2800$ die out at $R_a \simeq 300{,}000$ after the flow has made many transitions towards wavenumber 1. This loss of turbulence at high R_a is an artifact of the 2-D model, which will break down if R_a is made too large while β is held fixed. Such behavior was seen in the spherical laboratory experiments of Hart et al. 1986 that show strong 3-dimensional convection in this limit.

vi) The model appears to be reasonably self-consistent over most of its parameter range. The basic expansion requires that the Rossby number be small. The root mean square value of R_o over space and time is $\bar{R}_o = G\omega_{rms}/\beta$, where ω is the local nondimensional vorticity in the solutions. As shown in §2 the parameter G is geometrically related to the actual topographic slope in figure 1 by

$$G = 2\,\frac{\tan(\eta)D}{L} = 2\,\frac{\cot(\theta)D}{L} \simeq O(1) \qquad (17)$$

for a planetary atmosphere at subtropical latitudes θ (see also eqn. 8′). Setting G = 1, at $R_a = 10^6$ we find, for example, that $\bar{R}_o$ falls below one for $\beta > 6000$ and below one tenth for $\beta > 10^4$.

Horizontal non-divergence of the lowest order velocity field requires that

$$1 >> \frac{g\alpha T^{*}\cdot}{2\Omega U^{*}} = R_a \frac{G}{\beta}\,\frac{T}{U} \,. \qquad (18)$$

Using time and space averaged values for temperature T and velocity U, this condition is well satisfied by our solutions. For example, at $R_a = 5\times10^6$ the RHS of (18) is 0.071 at $\beta = 4000$, decreasing to 0.021 at $\beta = 20{,}000$.

On a spherical planet thermal winds giving a variation of velocity along the axis of rotation will be induced by the component of gravity g_p parallel to the rotation axis. Combining this component with the slopes η appropriate to a sphere yields an estimate of the fractional change of velocity over the depth D be small. This is

$$\epsilon = \frac{2R_a}{\beta U}\,|\nabla T| \,, \qquad (19)$$

since $LGg_p/gD \simeq 2D\tan(\theta)/L \cdot \cot(\theta)L/D = 2$. Computations of $(\nabla T.\nabla T)^{1/2}/(\mathbf{v}.\mathbf{v})^{1/2}$ indicate that the ϵ is rarely above 1/2 except at special points where the speed is zero. Thus the computed flows appear approximately consistent with the model assumptions provided one is in the β-convection regime. We expect some quantitative corrections when ageostrophic and thermal wind effects are included. At values of $\beta <\simeq \beta_v$ the solutions may be quite unrealistic for situations with $G \simeq O(1)$. However, these latter motions could be observed in a laboratory centrifugal annulus experiment with almost horizontal ends ($\eta \to 0$) so that G becomes very small.

vii) The basic model is too simplistic for a direct quantitative comparison with planetary and stellar atmospheres as it neglects full sphericity, compressibility, as well as other potentially important thermodynamic effects. Nonetheless, it is tempting to speculate that Jovian dynamics are associated with a turbulent flow having a β near to β_v, and that the convection zone on the Sun is associated with flow near to β_m. This puts Jupiter in a low-wavenumber eddy state associated with a strong quasi-steady zonal flow. The Sun is represented by a higher wavenumber eddy state with a pulsating zonal flow (e.g. fig. 9c or 9d for Jupiter, fig. 9e or 12 for the Sun). Magalhaes et al. (1990) have deduced the presence of slow moving zonal wavenumber 9 - 11 eddies in thermal images of Jupiter. They suggest that these motions may be rooted many scale heights below the cloud deck. On the other hand, surface observations and helioseismology of

the interior of the Sun have not as yet exposed any low wavenumber giant cells, so we believe that the finer structure high-β convection may be more appropriate for this body.

After fixing the geometry and the Prandtl number, the model has two virtually unknown dimensional parameters, the small-scale eddy viscosity ν and the super-adiabatic buoyancy forcing $g\alpha\Delta T/D$ exciting the convection. Assuming a value of $R_a \simeq 10^7$ and $N_u \simeq 2$, we can obtain an small-eddy diffusion velocity for Jupiter by requiring that the model yield the observed internal convection flux F of about 5 watts/m^2. The diffusion velocity

$$\frac{\nu}{D} = \left\{ \frac{g\alpha DF}{\rho C_p R_a N_u} \right\}^{1/3} \tag{20}$$

obtained in this way is relatively insensitive to the various parameters. Taking $C_p = 1.4\times10^4$ joules/Kg$^\circ$K , $\alpha = 1/200^\circ$K , g = 20 m/sec^2 , ρ = 2 Kg/m^3, and $D = 2\times10^7$ m, we get $\nu/D \simeq .045$ m/sec. Setting G = 0.3 and using the rotation rate for Jupiter we get $\beta \simeq 48{,}000$. The results from table 1 then give a dimensional cross-channel zonal velocity difference of about 120 m/sec, which is roughly the same size as that observed. The model zonal shear fluctuates by about 15 percent on a timescale of 1.3 years. The zonal kinetic energy generation rate, 6.4×10^6, is about one third of the eddy kinetic energy generation by buoyancy work $R_aN_u \simeq 1.8\times10^7$. The former number translates to a dimensional value of 3×10^{-5} m^2/sec^3, which is somewhat smaller than the values reported from Voyager I of $(1 - 4)\times10^{-4}$ m^2/sec^3 (Ingersoll et al. 1981). It may be noted that Sorovsky et al. (1982) have argued that the actual correlation, after accounting for sampling bias, may be considerably smaller than this latter value. Nonetheless, the model efficiency of β-convection for generating zonal jets is quite high, with a substantial fraction of the buoyancy work going in maintenance of the zonal jets.

Carrying out the same procedure for conditions typical of the outer convection zone of the Sun with D equal to a solar radius gives a very large viscosity $\nu \simeq 1.3\times10^9$ m^2/sec. The associated $\beta \simeq 7500$ is below the β-convection regime at $R_a = 10^7$. If we take a value $\nu \simeq 10^8$ m^2/sec, which is about a third that estimated from surface magnetic feature diffusion and typical of values used in large eddy models of compressible convection on the Sun (Gilman and Miller, 1986), then $\beta \simeq 80{,}000$ and we are in the pulsating turbulence regime. The diffusion velocity is .14 m/sec and the dimensional zonal cross-channel velocity difference is about 300 m/sec, which is the observed scale of differential rotation between the equator and high latitudes. More interesting is the pulsation period, which turns out to be 13 years for these parameters. Might almost-periodic shear-convection interactions in a turbulent flow have something to do with the 11 year solar activity cycle? The demonstration of a dynamical mechanism for producing oscillations with a similar timescale is intriguing. However, this latter more realistic value of the viscosity, although yielding reasonable numbers for the differential rotation rate and the pulsation period, leads to a convective flux that is too small by a factor of a thousand. Leaving aside the question of flux partitioning between different transport

mechanisms and between various represented and non-represented eddy sizes, it is thought that a Prandtl number considerably smaller than one is more appropriate for the Sun. Low Prandtl number β-convection forced by thermal boundary fluxes or internal heating is an area for future study.

With respect to Jovian dynamics, a problem with the model is that it generates only one zonal shear zone, and multiple jets in y have not yet been found (though see fig. 6b for some wrinkles). Soward (1977) investigated the dynamics of small but finite-amplitude convection in an internally heated fluid sphere and concluded that meridional variations should appear on scales of order $\beta^{-2/9}$ as $\beta \to \infty$, which only becomes substantially less than one at the extreme values of β in our calculations. It is not clear how relevant this weakly nonlinear analysis is for the turbulent regime we are studying. For this situation Rhines (1975) has proposed that 2-D turbulence on a β-plane will cascade energy upscale into zonally symmetric modes with y-wavenumbers $k^*_\beta \simeq [\beta^*/2U^*rms]^{1/2}$, or equivalently, into non-dimensional cell sizes $l_\beta \equiv \pi/Dk^*_\beta \simeq 2^{3/4}\pi\, K'^{1/4}/\beta^{1/2}$. Using the data from table 1 it can be seen that l_β is of order 1 except for those runs with $\beta \to \beta_{lin}$ where the convection is only weakly turbulent. In order to study the possibility of multiple jet solutions we need to consider simulations at even higher R_a, perhaps as large as 10^{10} . Although the possibility of attaining flow statistics over a wider range of parameters is appealing, such simulations will require much higher resolution and very tiny time steps.

The two-dimensional β-convection model has allowed us to study flow evolution and equilibration at higher Rayleigh numbers and Taylor numbers ($\propto \beta^2$), and over much longer time scales, than is possible with a global eddy-resolving 3-D convection code. However, as computer parallelism and speed increase, it would be interesting to look for similar turbulent vacillation states in three dimensional compressible models of stellar and planetary atmospheres.

REFERENCES

Busse, F.H., "A simple model of convection in the Jovian atmosphere," *Icarus*, **29**, 255 - 260 (1976).

Busse, F.H., "A model of mean zonal flows in the major planets," *Geophys. and Astrophys. Fluid Dyn.*, **23** 153 - 174 (1983).

Busse, F.H., and Or, A.C., "Convection in a rotating cylindrical annulus: thermal Rossby waves," *J. Fluid Mech.*, **166**, 173 - 187 (1986).

Carrigan, C.R. and Busse, F.H., "An experimental and theoretical investigation of the onset of convection in rotating spherical shells," *J. Fluid Mech.*, **126**, 287 - 305 (1983).

Cattaneo, F., and Hart, J.E., "Multiple states for quasi-geostrophic channel flows," *Geophys. and Astrophys. Fluid Dyn.*, **54**, 1 - 33 (1990).

Gilman, P.A., and Miller, J., "Nonlinear convection of a compressible fluid in a rotating spherical shell," *Astrophys. J. Suppl.*, **61**, 585 - 608 (1986).

Hart, J.E., Glatzmaier, G.A., and Toomre, J., "Space-laboratory and numerical simulations of thermal convection in a rotating hemispherical shell with radial gravity," *J. Fluid Mech.*, **173**, 519 - 544 (1986).

Howard, L.N., and Krishnamurti, R., "Large-scale flow in turbulent convection: a mathematical model," *J. Fluid Mech.*, **170**, 385 - 410 (1986).

Howard, R., and Harvey, J., "Spectroscopic determinations of solar rotation," *Solar Phys.*, **12**, 23 - 51 (1970).

Ingersoll, A.P., Beebe, R.F., Mitchell, J.L., Garneau, G.W., Yagi, G.M., and Muller, J.P., "Interaction of eddies and mean zonal flow on Jupiter as inferred from Voyager 1 and 2 images," *J. Geophys. Res.*, **86** 8733 - 8743 (1981).

Ingersoll, A.P. and Pollard, D., "Motions in the interiors and atmospheres of Jupiter and Saturn: Scale analysis, anelastic equations, barotropic stability criterion," *Icarus*, **52**, 62 - 80 (1982).

Lilly, D.K., "Comments on 'Venus' s circulation is a merry-go-round," *J. Atmos. Sci.*, **28**, 827 - 828 (1971).

Lin, R.-Q., Busse, F., and Ghil, M., "Transition to two-dimensional turbulent convection in a rapidly-rotating annulus," *Geophys. and Astrophys. Fluid Dyn.*, **45**, 131 - 157 (1989).

Lin, R.-Q., "Double column instabilities in the barotropic annulus," *Geophys. and Astrophys. Fluid Dyn.*, **54**, 161 - 188 (1990).

Lipps, F.B., "Two-dimensional numerical experiments in thermal convection with vertical shear," *J. Atmos. Sci.*, **28**, 3 - 19 (1971).

Magalhaes, J.A., Weir, A.L., Conrath, B.J., Gierasch, P.J., and Leroy, S.S., "Zonal motion and structure in Jupiter' s upper troposphere from voyager infrared and imaging observations," *Icarus*, **88**, 39 - 72 (1990).

Moore, D.R., Weiss, N.O. and Wilkins, J.M., "Asymmetric oscillations in thermosolutal convection," *J.Fluid Mech.*, **233**, 561 - 585 (1991).

Moore, D.R., and Weiss, N.O., "Two dimensional Rayleigh-Benard convection," *J. Fluid Mech.*. **58**, 289 - 312 (1973).

Or, A.C. and Busse, F.H., "Convection in a rotating cylindrical annulus. Part 2. Transitions to asymmetric and vacillating flow," *J. Fluid Mech.*, **174**, 313 - 326 (1987).

Pedlosky, J., *Geophysical Fluid Dynamics*, Springer-Verlag, N.Y., 710pp., (1987).

Rhines, P.B., "Waves and turbulence on a β-plane," *J. Fluid Mech.*, **69**, 417 - 443 (1975).

Richtmyer, R.D., and Morton, K.W., *Difference methods for initial value problems*, Interscience, (1967).

Schnaubelt, M., and Busse, F.H., "Convection in a rotating cylindrical annulus with rigid boundaries," *Nonlinear Evolution of Spatio-Temporal Structures in Dissipative Continuous Systems*, F.H. Busse and L. Kramer Ed., 67 - 72 (1991).

Schnaubelt, M., "Stationare und Zeitabhangig Konvektion im Rotierenden Zylindrischen Annulus," Ph.D. Thesis, Univ. Bayreuth, 80p. (1992).

Smith, G.D., *Numerical solution of partial differential equations*, Oxford Mathematics Handbooks, (1965).

Sorovsky, L.A., Revercomb, V.E., Suomi, V.E., Limaye, S.S., and Krauss, R.J., "Jovian winds from Voyager 2. Part II: Analysis of eddy transports," *J. Atmos. Sci.*, 39, 1433 - 1455 (1982).

Soward, A. M., "On the finite amplitude thermal instability of a rapidly rotating fluid sphere," *Geophys. and Astrophys. Fluid Dyn.*, 9, 19 - 74 (1977).

Thompson, R.O.R.Y., "Venus's circulation is a merry-go-round," *J. Atmos. Sci.*, 27, 1107 - 1116 (1970).

FIGURE CAPTIONS

Fig. 1. Geometry of the equatorial channel model. The channel has width D and height L. Gravity is assumed perpendicular to the rotation axis.

Fig. 2. Properties of linear instabilities. (a) Critical Rayleigh number vs. zonal wavenumber (lowest cross-stream mode) for values of β shown. (b) Growth rate Re(s) for various β at $R_a = 10^6$.

Fig. 3. Typical wavenumber spectra of nonlinear solutions. $\beta = 2800$. (a) Symmetric wavenumber 1, $R_a = 42{,}500$. (b) Asymmetric wavenumber 1, $R_a = 75000$, with comparable energies in low and moderate wavenumbers. (c) Asymmetric type 2A(6) with dominant wavenumber 6, $R_a = 57500$. (d) Asymmetric type 8A, $R_a = 40000$.

Fig. 4. State diagram for $\beta = 2800$, tracking various wavenumber and symmetry states vs. Rayleigh number. Each horizontal line represents a solution branch with F = steady amplitude travelling waves (fixed point in energy), L = limit cycle, L2 = period-doubled cycle, T = two-frequency torus, T2 = period-doubled 2-torus, C = chaos. Single-tipped arrows denote changes upon increasing Rayleigh number using the last timestep of the previous solution as the initial condition. Double-tipped arrows denote evolution upon small amplitude perturbations ($\simeq$1 percent) with no symmetry.

Fig. 5. Results along the Type 8A branch. $\beta = 2800$. (a) $R_a = 57{,}500$. (b) $R_a = 75{,}500$. (c) $R_a = 76{,}000$. (d) $R_a = 125{,}000$. Vertical columns from left to right show area-averaged zonal kinetic energy vs. its rate of change, Poincare' sections of the phase plots, time series of zonal kinetic energy, and frequency spectra of the times series.

Fig. 6. Eddy ($m \neq 0$) streamfunction and zonal velocity vs. time for a) case

corresponding to Fig. 5a. b) corresponding to Fig. 5d. For this and all shaded pictures the gray scale spans the range of negative or minimum (black), to positive or maximum (white) values.

Fig. 7. Results along the Type 1S (unstable) branch. $\beta = 2800$. (a) $R_a = 43{,}000$. (b) $R_a = 43{,}250$. (c) $R_a = 43{,}600$. (d) $R_a = 43{,}750$. The structure of the diagram is the same as Fig. 5.

Fig. 8. Total streamfunction and horizontal wavenumber spectra for the multiple states at $R_a = 60{,}000$, $\beta = 2800$. (a) The chaotic type 1A(6) mode. (b) the steady amplitude travelling wave 1A(7) mode.

Fig. 9. Times series of eddy ($m \neq 0$) streamfunction at $R_a = 10^6$. (a) $\beta = 0$. (b) $\beta = 6000$ (ordinary convection branch). (c) $\beta = 6000$ (β-convection branch). (d) $\beta = 8000$. (e) $\beta = 20{,}000$. (f) $\beta = 28{,}000$. Coloration spans the range of negative (black) to zero (red) to positive (white) values.

Fig. 10. Dominant wavenumbers at $R_a = 10^6$. The crosses indicate spectral peaks, while the squares show the wavenumber of maximum linear growth rate.

Fig. 11. Variation of space averaged zonal kinetic energy and Nusselt number with time for the large zonal jet cases from figure 9 at $R_a = 10^6$. The Nusselt number is $\partial\overline{T}/\partial y$ at $y = 0$.

Fig. 12. Pulsating zonal jets and turbulent convection at $R_a = 10^7$, $\beta = 75{,}000$. Total streamfunction and non-conductive temperature are illustrated with the color scale as in figure 9.

Fig. 13. Time series of total mean kinetic energy and the pointwise zonal velocity at $y = 0.6667$ for the case shown in figure 12. The Nusselt number here is $\frac{\partial\overline{T}}{\partial y}$ at $y = 0$. The portions between the vertical dashed lines are illustrated in figure 12.

Fig. 14. Ratio of time averaged mean flow kinetic energy to time averaged eddy kinetic energy over the whole channel for the R_a values shown. The horizontal portions, past the β-cutoff (the short dashed curve), show the zero-lines for these offset plots. The long-dash curve indicates the transition from ordinary convection with very weak mean flows to those with large zonal jets. The narrow window of hysteresis in the transition is illustrated for $R_a = 10^6$.

Fig. 15. Qualitative regime diagram showing locations of pure conduction ("stable"), β-convection with large zonal jets, and "ordinary" stationary or travelling Rayleigh-Benard convection with small or zero (if $\beta = 0$) zonal flows. The asterisk points locate parameters where the largest zonal jets are found, subject to our fairly coarse parameter space sampling. The time-average cross-channel velocity differences are indicated.

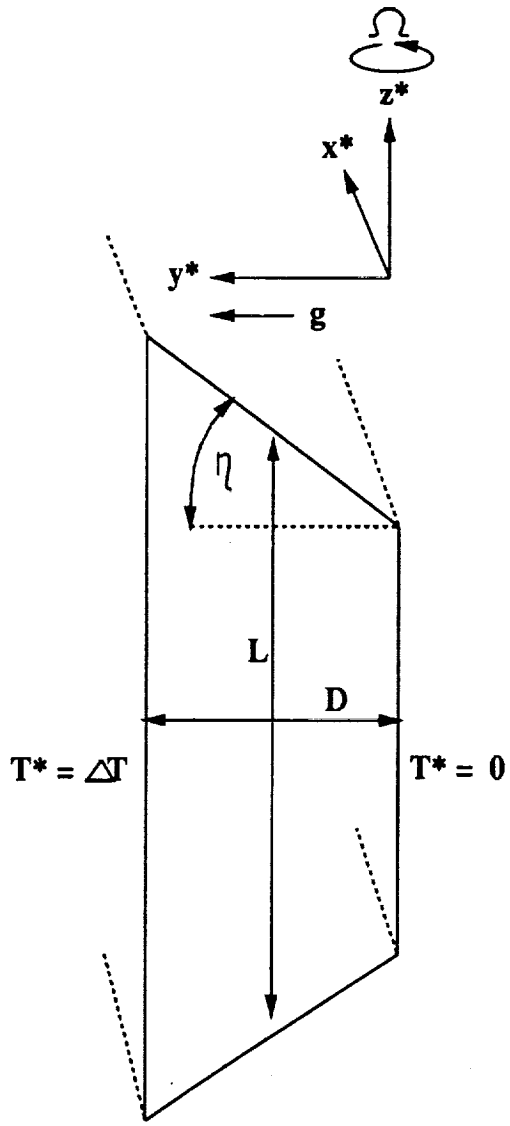
z*
x*
y*
g
η
L
D
T* = ΔT
T* = 0

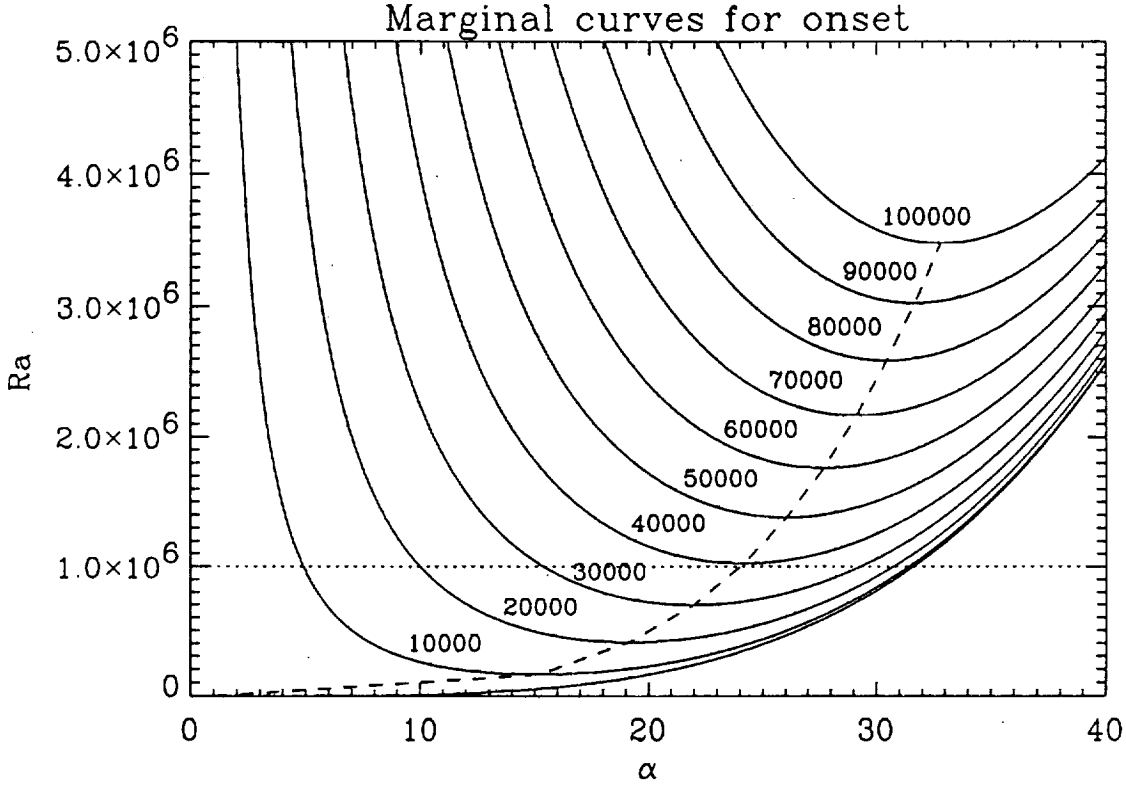
Marginal curves for onset
Ra
5.0×10^6
4.0×10^6
3.0×10^6
2.0×10^6
1.0×10^6
0
100000
90000
80000
70000
60000
50000
40000
30000
20000
10000
0
10
20
30
40
α

2a

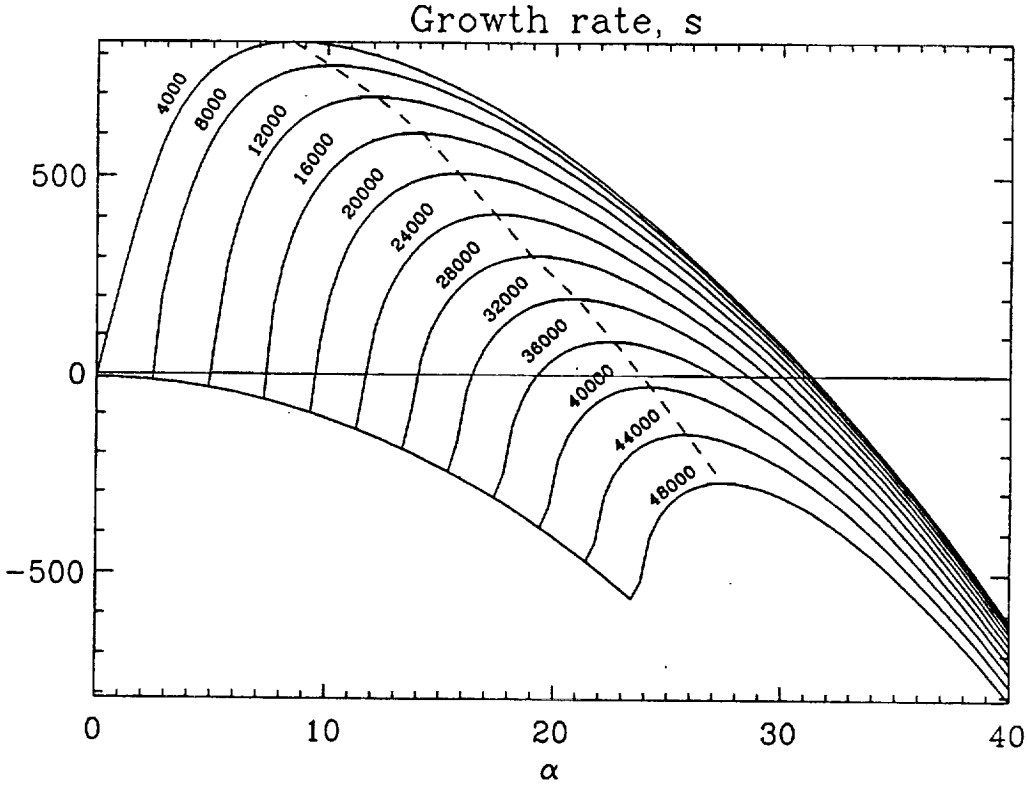
Growth rate, s
500
0
-500
4000
8000
12000
16000
20000
24000
28000
32000
36000
40000
44000
48000
0
10
20
30
40
α

2b

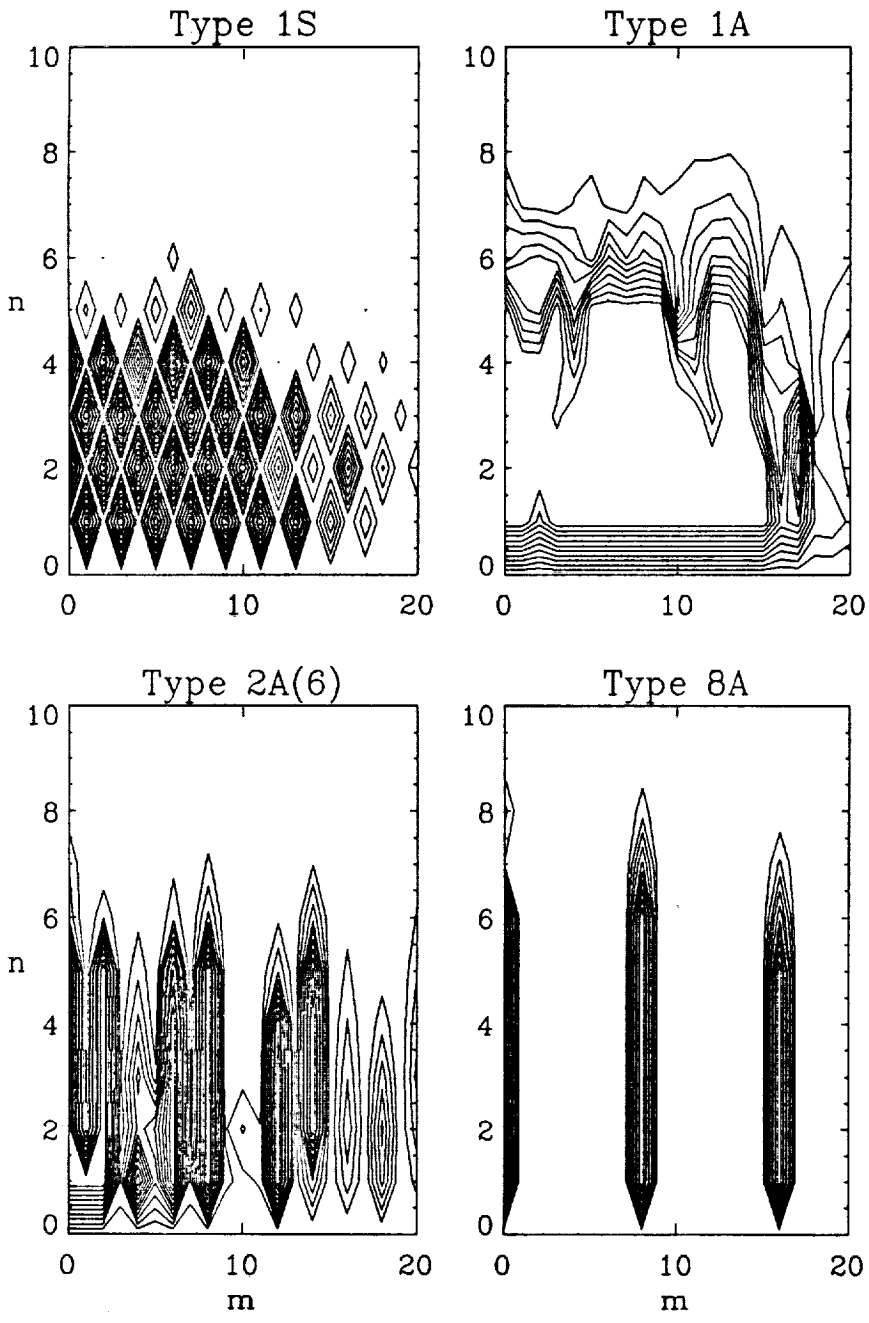
Type 1S
Type 1A
Type 2A(6)
Type 8A
n
m
0
2
4
6
8
10
20

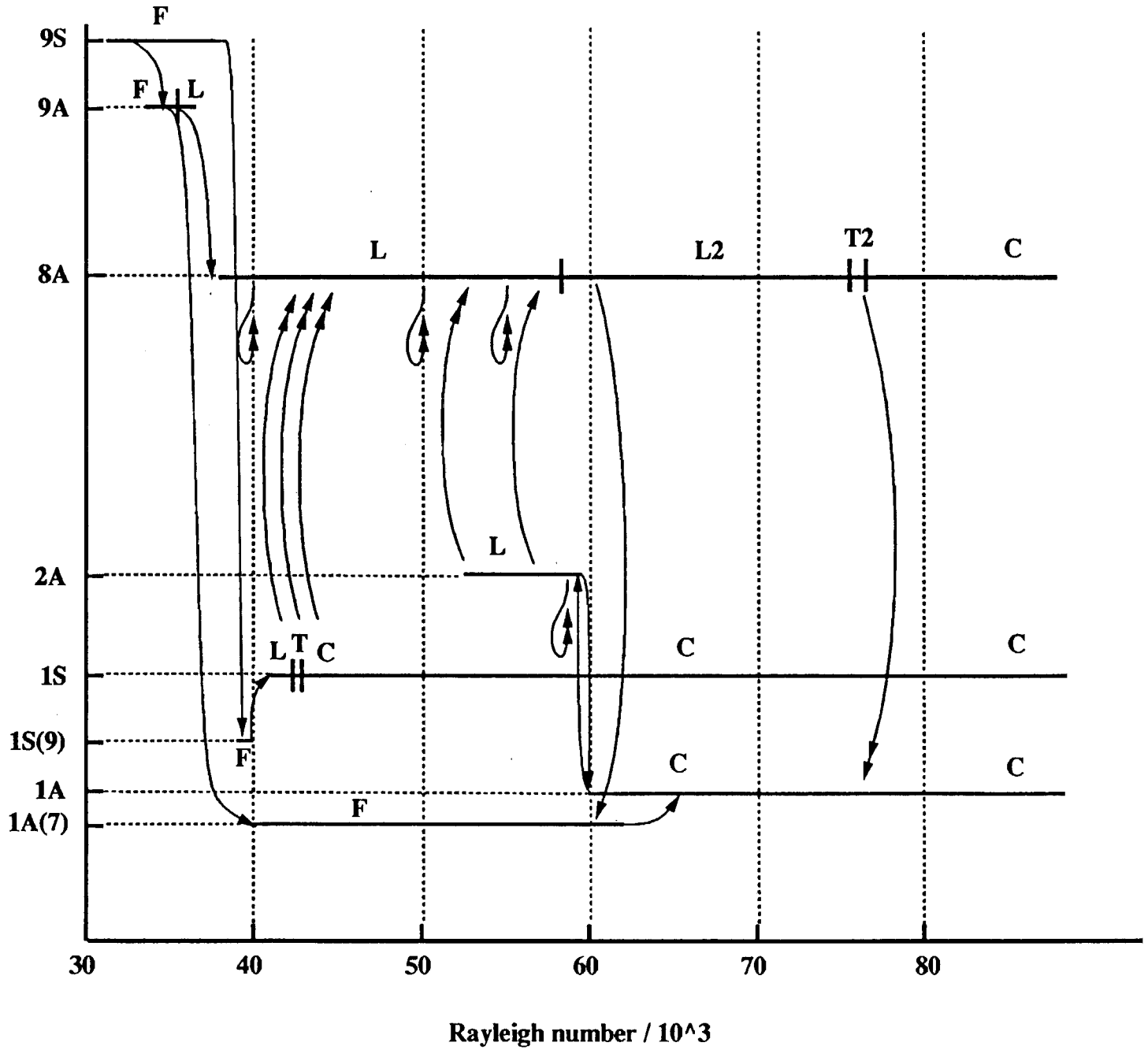
F
9S
F
L
9A
L
L2
T2
C
8A
L
2A
L T C
C
C
1S
1S(9)
F
C
C
1A
F
1A(7)
30
40
50
60
70
80
Rayleigh number / 10^3

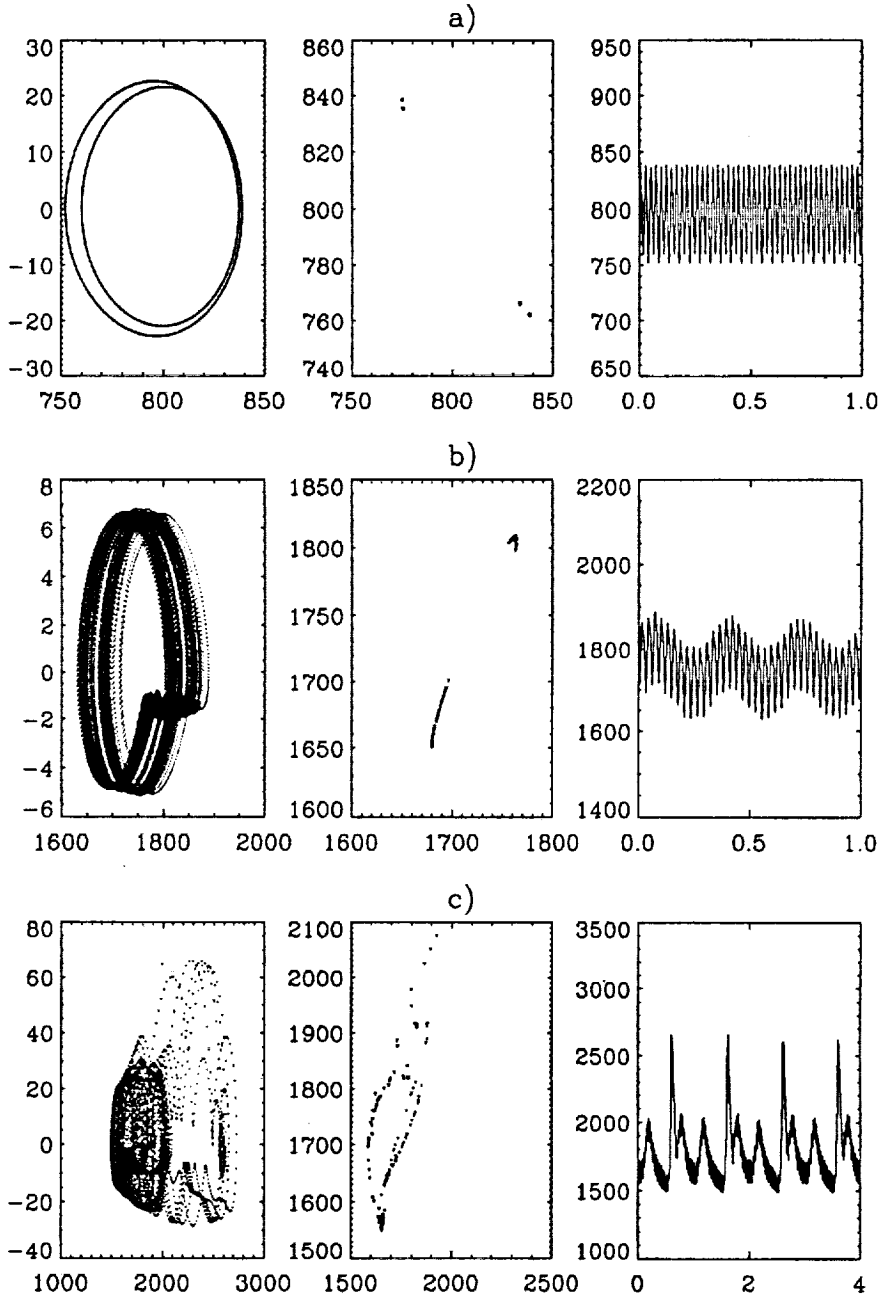
a)
30
20
10
0
−10
−20
−30
750
800
850
860
840
820
800
780
760
740
750
800
850
950
900
850
800
750
700
650
0.0
0.5
1.0
b)
8
6
4
2
0
−2
−4
−6
1600
1800
2000
1850
1800
1750
1700
1650
1600
1600
1700
1800
2200
2000
1800
1600
1400
0.0
0.5
1.0
c)
80
60
40
20
0
−20
−40
1000
2000
3000
2100
2000
1900
1800
1700
1600
1500
1500
2000
2500
3500
3000
2500
2000
1500
1000
0
2
4

6a

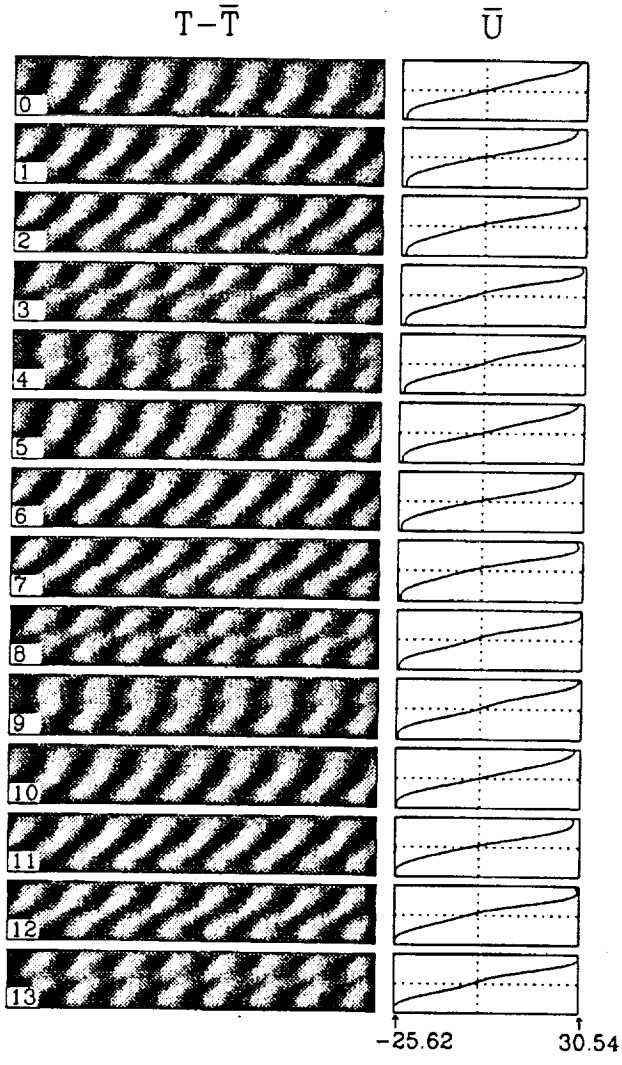
T−T̄
Ū
0
1
2
3
4
5
6
7
8
9
10
11
12
13
−25.62
30.54

6b

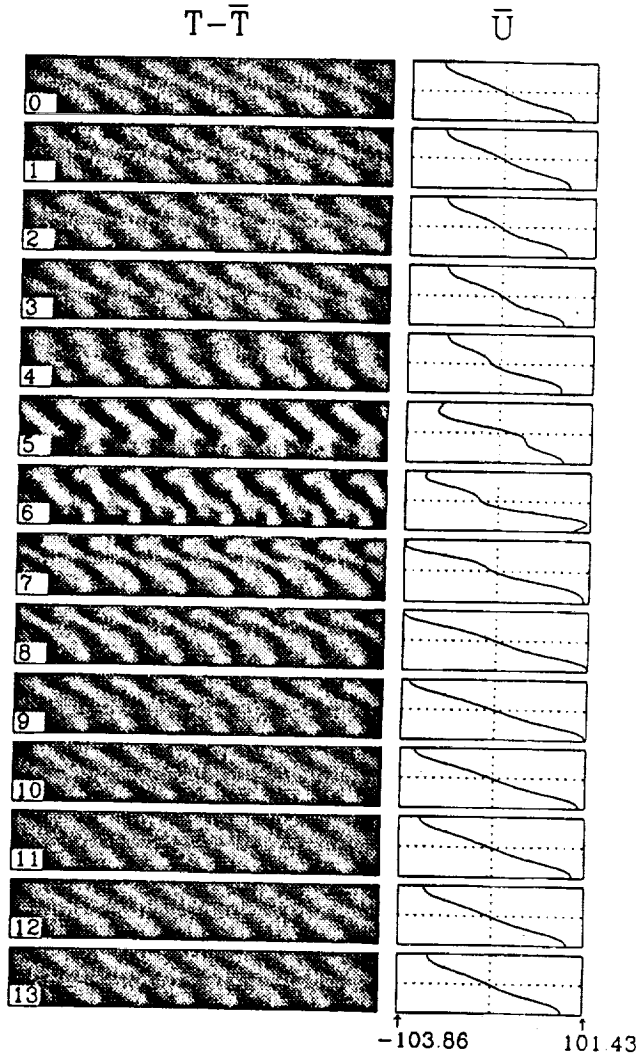
T−T̄
Ū
0
1
2
3
4
5
6
7
8
9
10
11
12
13
−103.86
101.43

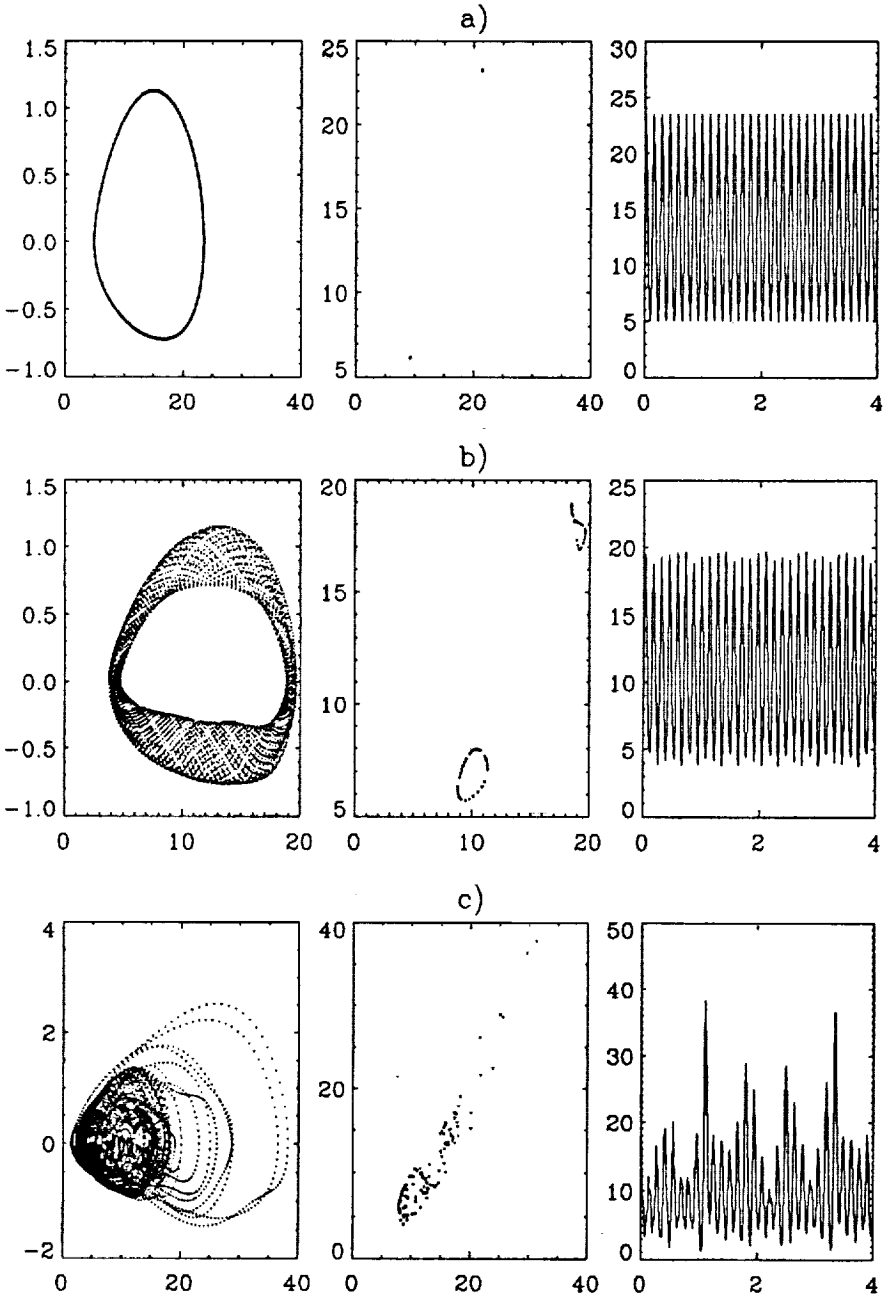
a)
1.5
1.0
0.5
0.0
−0.5
−1.0
0
20
40
25
20
15
10
5
0
20
40
30
25
20
15
10
5
0
0
2
4
b)
1.5
1.0
0.5
0.0
−0.5
−1.0
0
10
20
20
15
10
5
0
10
20
25
20
15
10
5
0
0
2
4
c)
4
2
0
−2
0
20
40
40
20
0
0
20
40
50
40
30
20
10
0
0
2
4

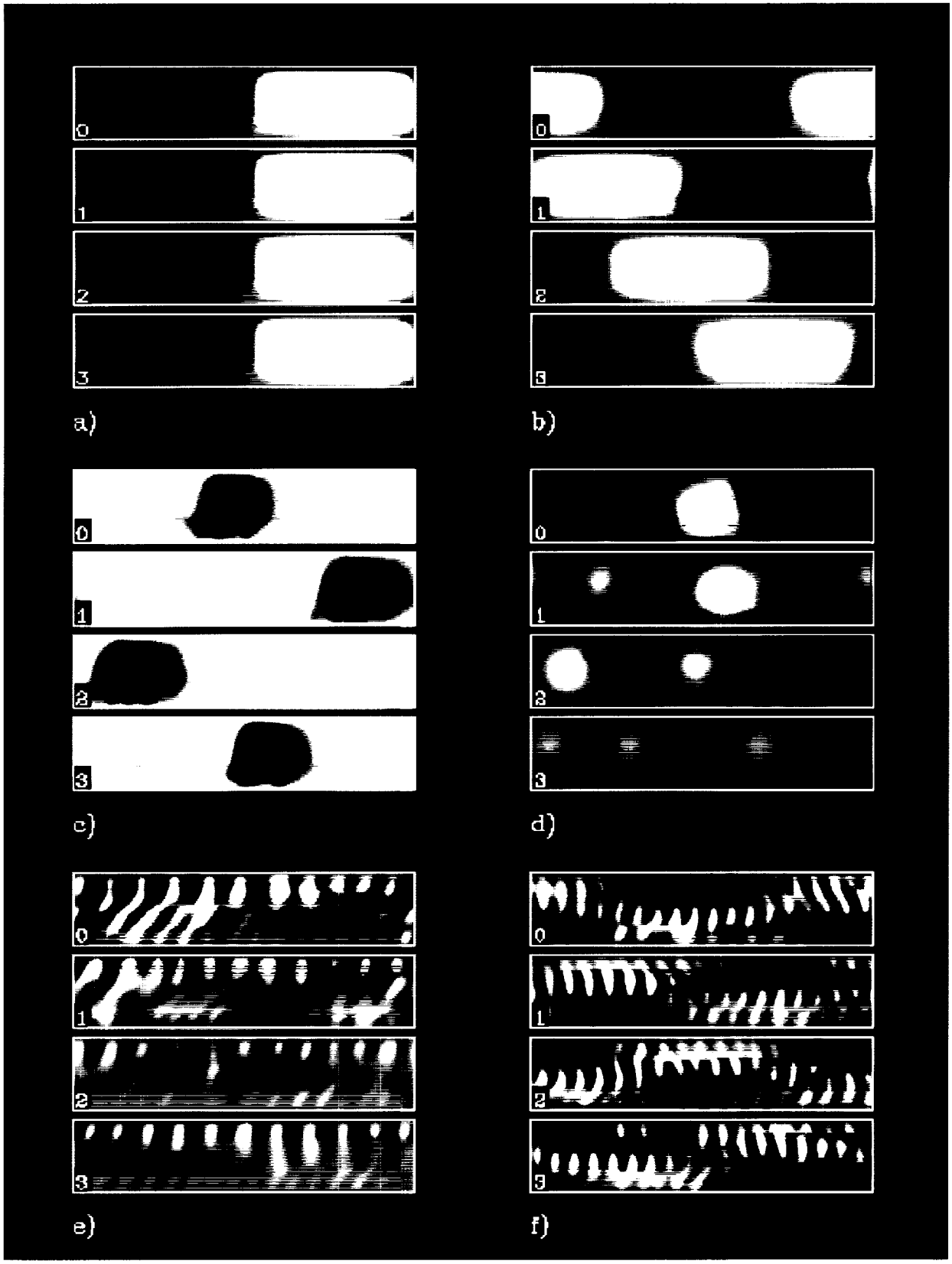

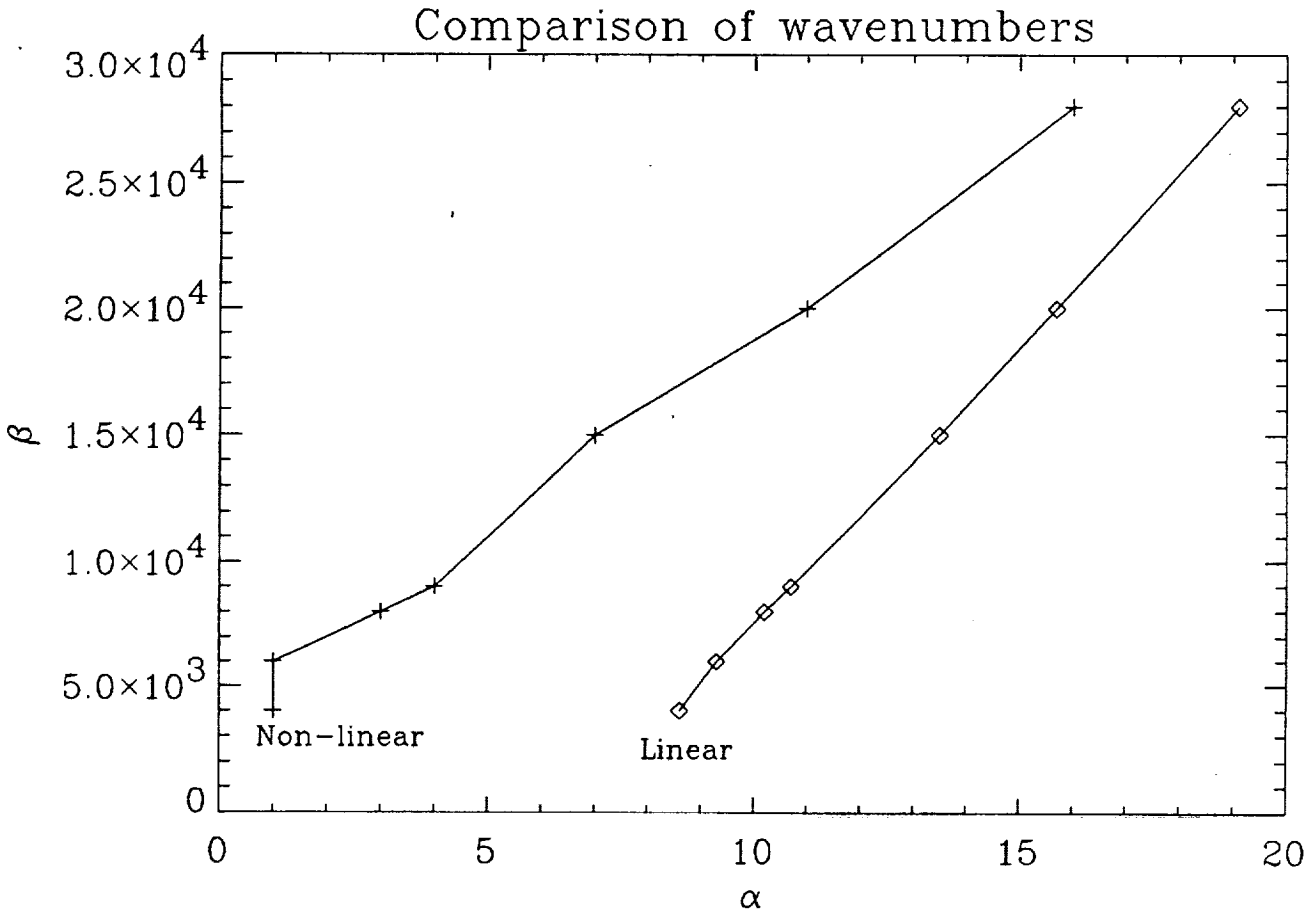
Comparison of wavenumbers
3.0×10^4
2.5×10^4
2.0×10^4
1.5×10^4
1.0×10^4
5.0×10^3
0
β
0
5
10
15
20
α
Non-linear
Linear

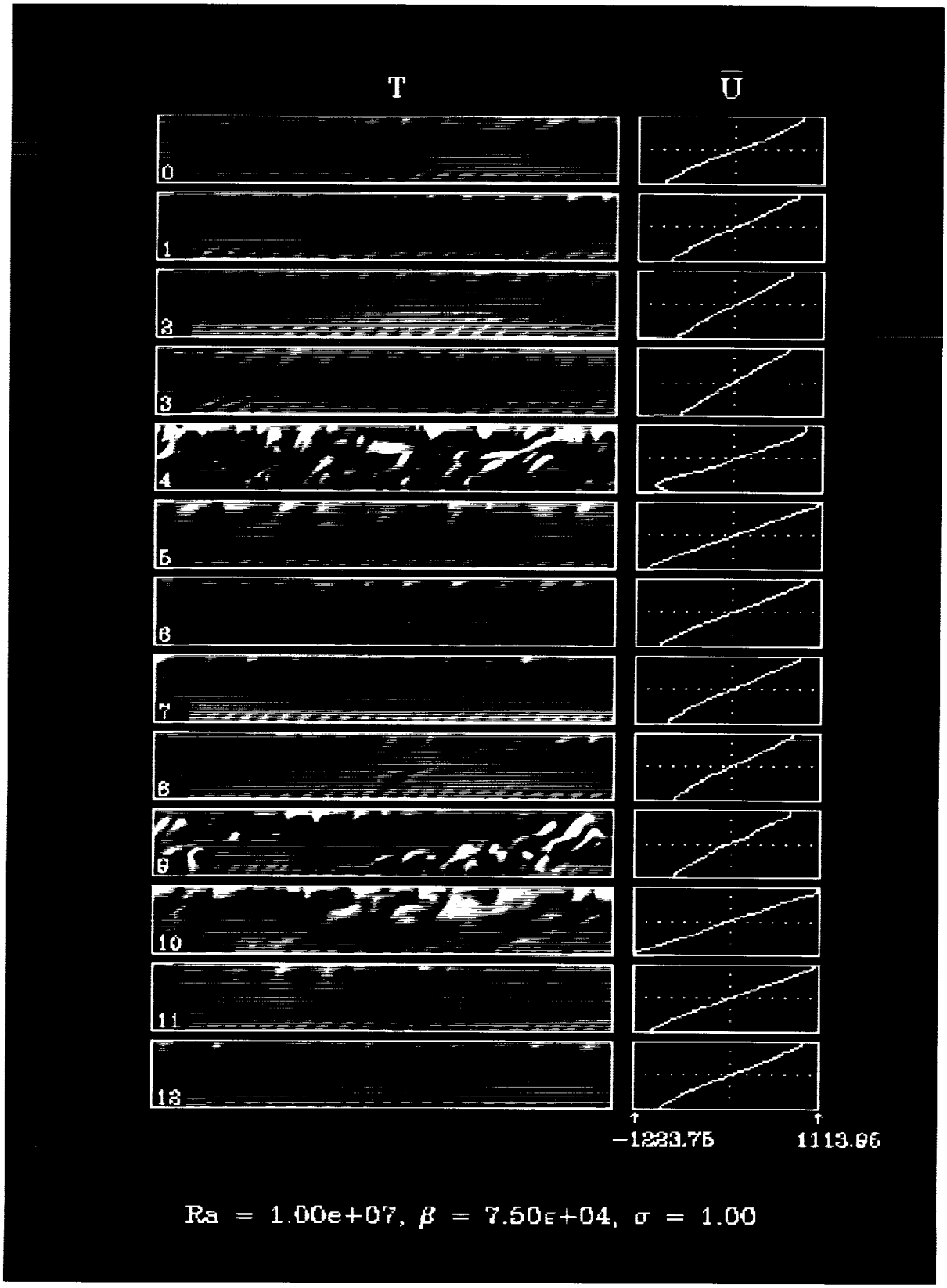

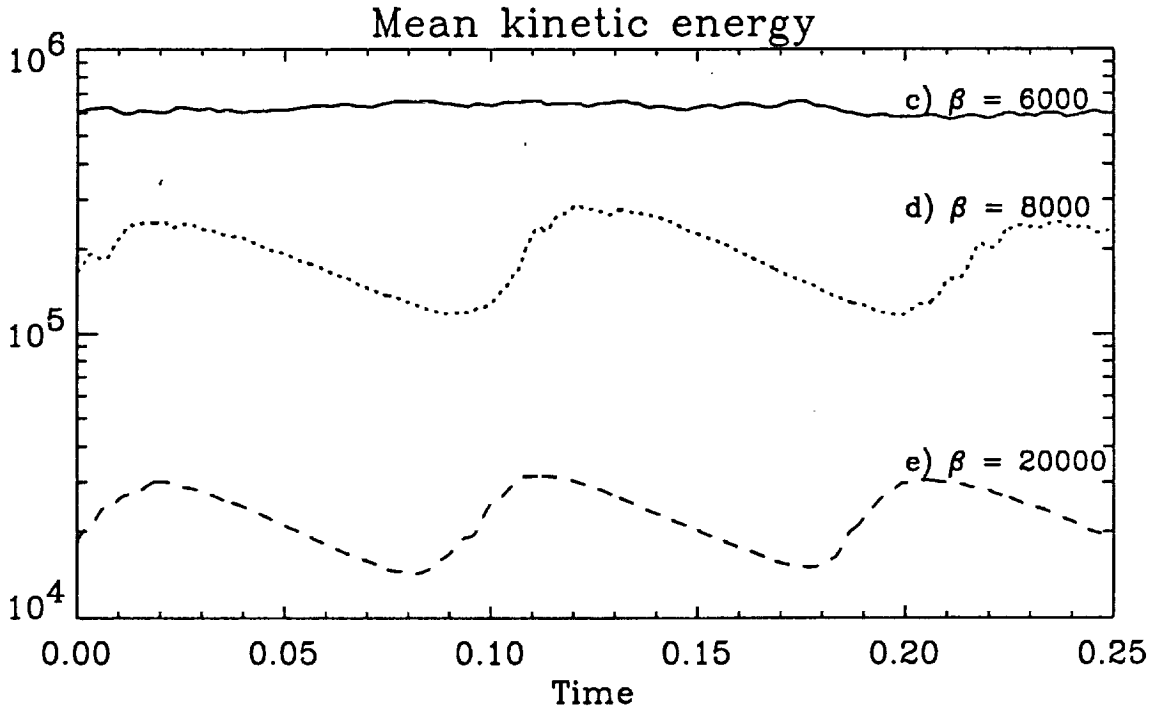
Mean kinetic energy
10^6
10^5
10^4
c) β = 6000
d) β = 8000
e) β = 20000
0.00
0.05
0.10
0.15
0.20
0.25
Time

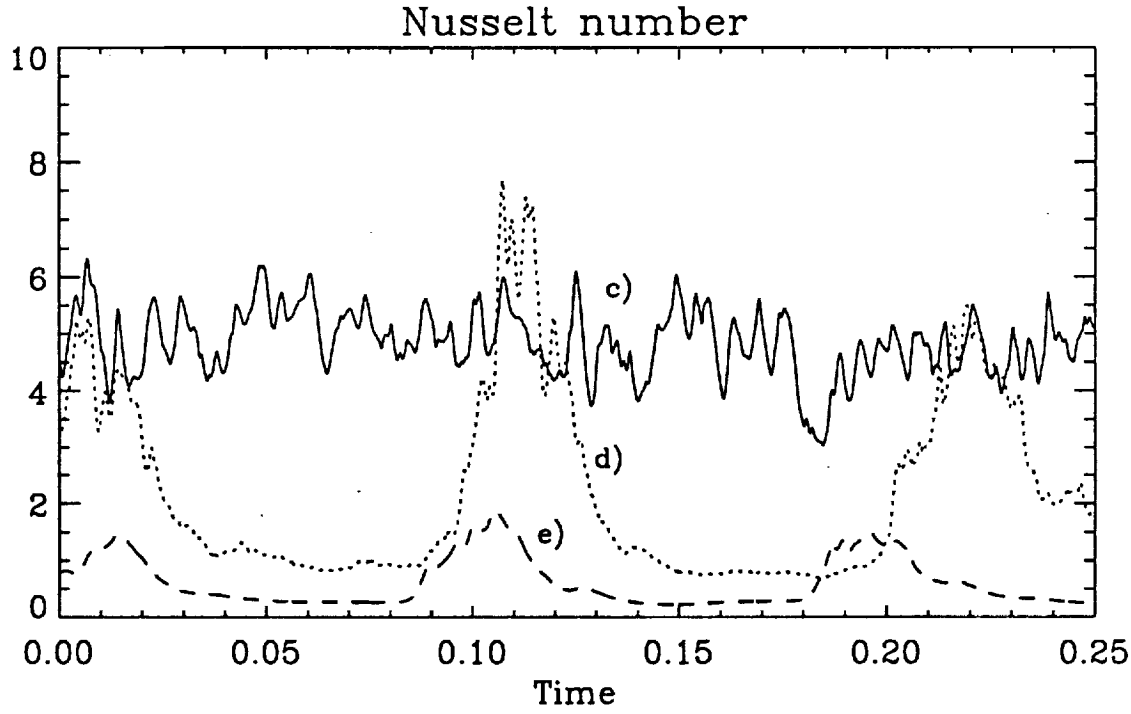
Nusselt number
10
8
6
4
2
0
c)
d)
e)
0.00
0.05
0.10
0.15
0.20
0.25
Time

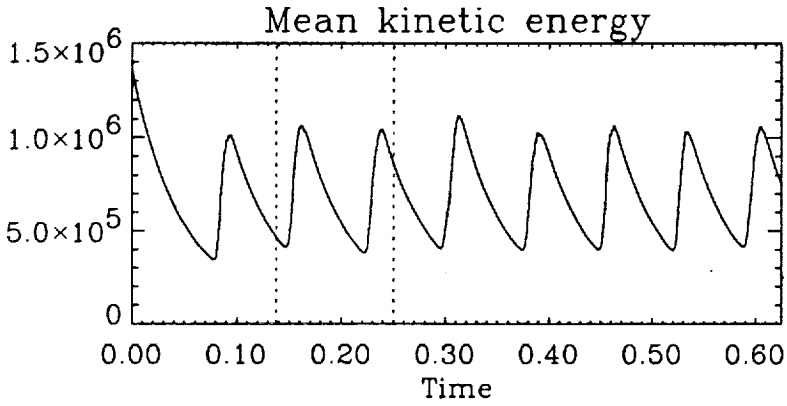
Mean kinetic energy
1.5×10^6
1.0×10^6
5.0×10^5
0
0.00
0.10
0.20
0.30
0.40
0.50
0.60
Time

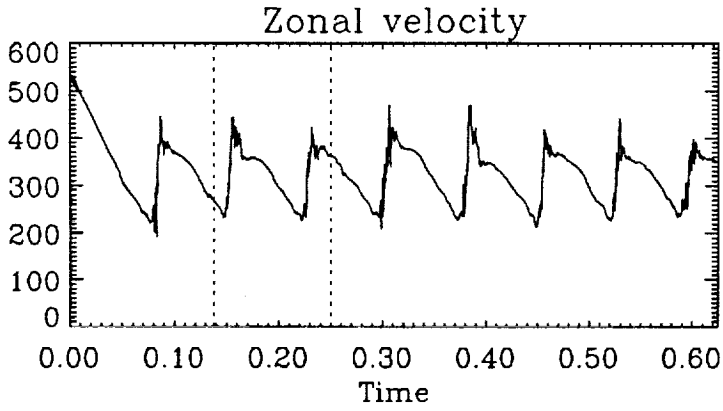
Zonal velocity
600
500
400
300
200
100
0
0.00
0.10
0.20
0.30
0.40
0.50
0.60
Time

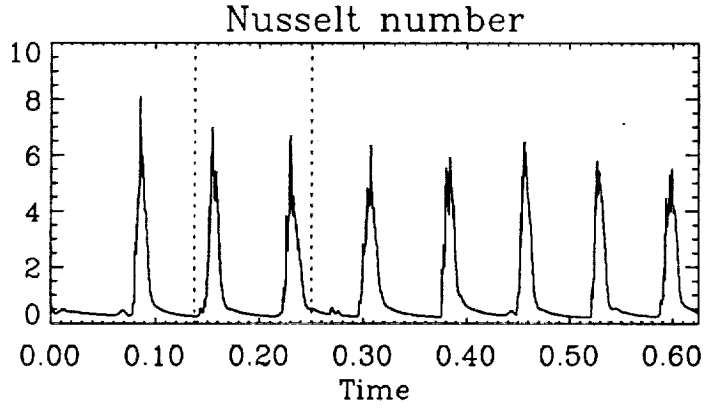
Nusselt number
10
8
6
4
2
0
0.00
0.10
0.20
0.30
0.40
0.50
0.60
Time

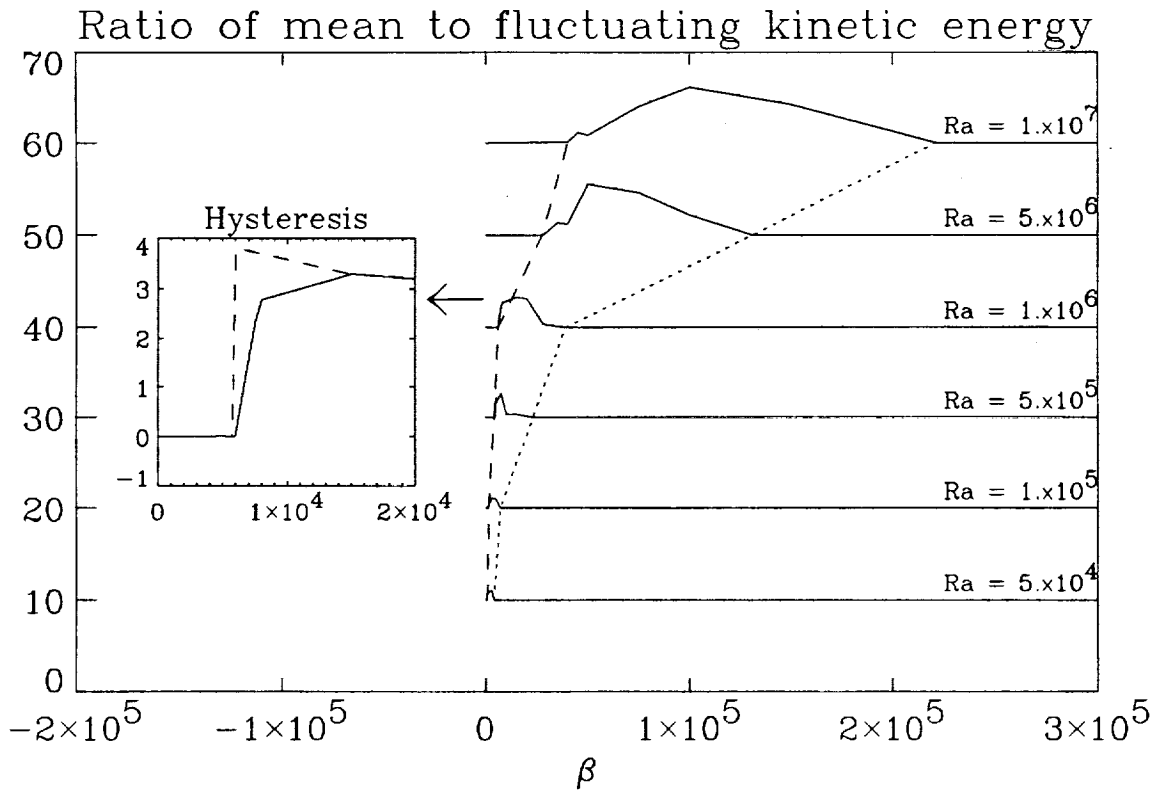
Ratio of mean to fluctuating kinetic energy
Hysteresis
Ra = 1.x10^7
Ra = 5.x10^6
Ra = 1.x10^6
Ra = 5.x10^5
Ra = 1.x10^5
Ra = 5.x10^4
β

Fig 14.

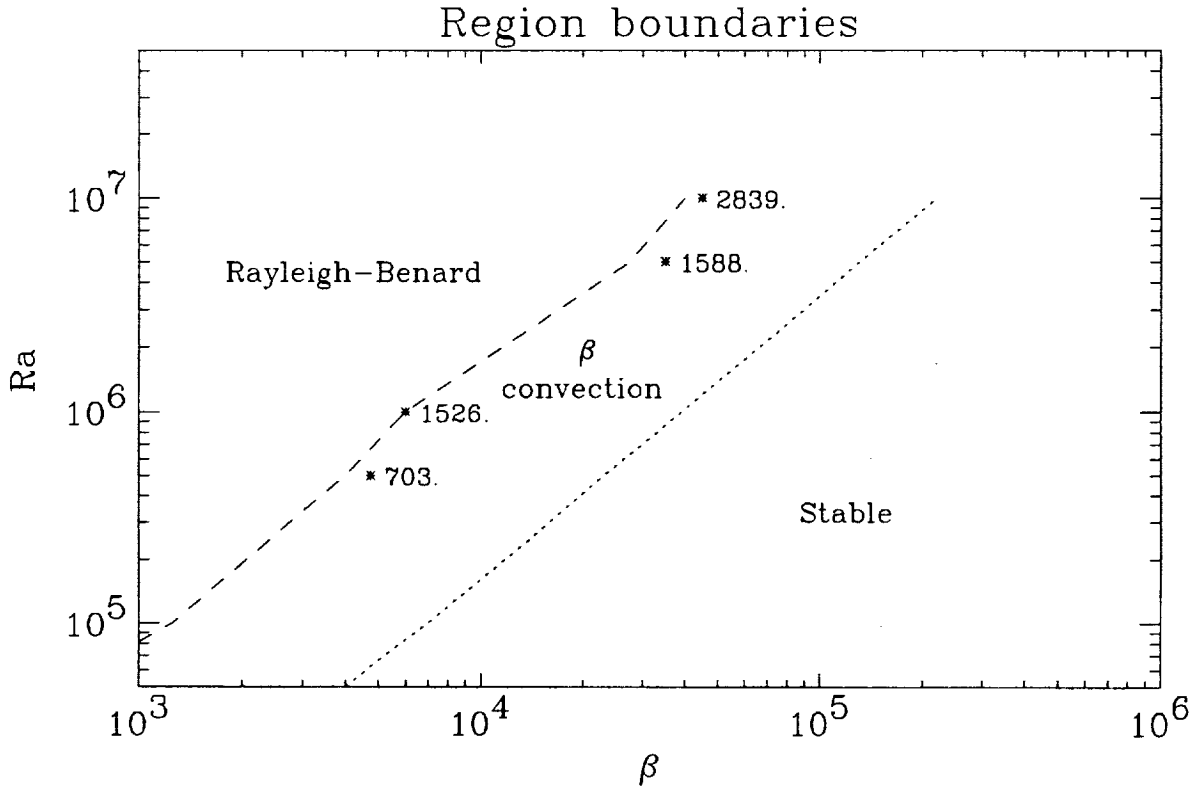
Region boundaries
Rayleigh–Benard
β
convection
Stable
2839.
1588.
1526.
703.
Ra
β

Fig 15.